A STUDY ON THE 9-MeV TOTAL SKIN ELECTRON THERAPEUTIC TECHNIQUE

A Thesis

Submitted to the Graduate Faculty of the
Louisiana State University and
Agricultural and Mechanical College
in partial fulfillment of the
requirements for the degree of

Master of Science

in

Nuclear Science
(Medical Radiation Science Option)

by

Jeffrey Paul Kurr
B.S., Northeast Louisiana University, 1978
May, 1991

ACKNOWLEDGMENTS

It has been a special privilege to receive training and instruction at the Mary Bird Perkins Cancer Center. The encouragement and support received from the staff is greatly appreciated. I am fortunate to have worked and studied under the guidance of Dr. Oscar Hidalgo-Salvatierra, Head of Physics and Vice President of Mary Bird Perkins Cancer Center. Also, special thanks are extended to Dr. Sheldon Johnson, and Carrie Rudolf, M.S.,of the Mary Bird Perkins Cancer Center, and Dr. Edward N. Lambremont of the Nuclear Science Center at Louisiana State University for serving on my committee. Thanks go to John Paul Luckett, M.S.,of the Mary Bird Perkins Cancer Center for reviewing my thesis. The support and advice received from Dr. Ray Wilenzick of Ochsner Clinic, New Orleans, is deeply appreciated. I am especially grateful to Penny Culley of the Baton Rouge Tumor Registry for her assistance and access to the SAS/STAT computer program. A special word of thanks goes to Yvonne Thomas for typing the thesis through several revisions.

Most of all, I am extremely thankful to Karen, my wife, for being a constant source of love and encouragement. I wish to express my gratitude to my father and mother, Paul and Mary Lee Kurr, for their love and for instilling within me patience and perseverance without which graduate research is impossible.

TABLE OF CONTENTS

TABLE OF CONTENTS, CONTINUED

TABLE OF CONTENTS, CONTINUED

LIST OF TABLES

LIST OF FIGURES

LIST OF FIGURES, CONTINUED

LIST OF FIGURES, CONTINUED

ABSTRACT

Dosimetric parameters have been determined for a total skin electron therapeutic technique utilizing 9 MeV electrons from a Varian Clinac 18 linear accelerator at Mary Bird Perkins Cancer Center. Beam parameters have been determined for both horizontal and angulated beams using both water and polystyrene phantoms. However, the delivery of an acceptable, vertically uniform dose to a patient at a 320 cm source-to-skin distance requires treatments to be given with angulation of the gantry 19^0 above the horizontal and 19.6^0 below the horizontal to comprise one dual field. The greatest variation in relative dose to clinically significant points in the treatment plane was 9%. The factors necessary for monitor unit calculation from a prescribed dose are described. The factor in this monitor unit calculation which presented the greatest contribution to the overall error was the fractional contribution of a dual field. The electron dosage to any point on a patient was estimated and shown to be delivered from only three of the six dual fields which compose the entire treatment cycle. The dosage from the photon contamination existing within the electron beam resulted from all six dual fields and was calculated to be 2.3% with this technique. Oblique surfaces were responsible for a superficial shift in the depth of a maximum dose to at least 4 mm from the surface. The therapeutic depth (d_{90}) was shown to be 8 mm.

Dosimetry parameters for cones with scattering panels attached to their distal apertures and having a 100 cm source-to-surface distance displayed insignificant differences with changes in cone size and scattering material. The insertion of a

scattering panel resulted in superficial shifts of the depth parameters by an amount roughly equal to the thickness of the scattering panel.

INTRODUCTION

High energy electrons are known for their sharp dose reduction and shallow energy deposition. Shallow energy deposition makes possible the treatment of superficial diseases without significant dose to the underlying structures. The utility of electrons in the treatment of extensive superficial tumors has been known since 1953. From the dosimetric point of view, the goal of total skin electron therapy is the delivery of a uniform dose to the whole skin area (Trump et al. 1953). Many techniques have been presented in the literature since that time, each striving toward the delivery of a uniform dosage to the entire skin surface. Because beta particles from radioactive sources have proven inadequate in regard to both exposure time and penetration due to inhomogeneity (Haybittle 1965; Trump 1953), and because of the variable electron energies available with the use of linear accelerators in total skin electron therapy, the utilization of linear accelerators is clearly preferred.

The techniques developed utilizing the linear accelerator include the translation of patients beneath narrow rectangular electron beams (Trump 1953), a horizontal single or multifield electron beam technique (Tetenes and Goodwin 1977), a paired parallel beam technique (Szur et al. 1962), a dual field or a paired, angled electron beam technique (Karzmark et al. 1960; Karzmark 1964; Page et al. 1970), the pendulum-arc technique (Sewchand et al. 1979), and patient rotation in both a single horizontal beam (Tetenes and Goodwin 1977) and in dual fields (Kumar et al. 1987). Kumar et al. (1987) describes the superiority of both the

rotational and an eight field technique over the six field technique with respect to dose homogeneity. The greater the number of fields utilized in a given technique, the greater the dose homogeneity and the lesser the overall penetration of the electrons when compared to the penetration of a single field (Bjarngard et al. 1977). A decreased percent depth dose is observed with obliquely incident beams and this effect increases with increased angulation and decreased energy of the beam (Biggs 1984; Ekstrand and Dixon 1982). Patient self-shielding that occurs in the superficial concavities of the body due to the oblique incidence of the electrons in these areas remains, but is reduced with patient rotation (Tetnes and Goodwin 1977; AAPM 1988). Trump et al. (1953) states that the range of electrons is proportional to the voltage utilized and that the tumoricidal depth may be customized to the depth of the tumor. Coffey et al. (1982) utilized a variable energy technique in the treatment of mycosis fungoides. Nine (9) MeV electrons were used until the involved areas of the skin became smooth and then 6 MeV electrons followed for the remainder of the treatment.

The Mary Bird Perkins Cancer Center in Baton Rouge, Louisiana, has expressed the need for a 9-MeV total skin electron technique for those patients with disease extending deeper into the body than the tumoricidal depth available with a 6-MeV technique.

The total skin electron therapy technique in present use is a technique similar to that presented by Page et al. (1970). A polystyrene scattering panel having the dimensions of 100 cm x 212 cm x 0.635 cm is located two meters away

from the isocenter of an isocentrically mounted Varian Clinac 18 linear accelerator. The polystyrene scatterer also serves as an energy degrader. No electron cone is used. The field size is opened to 35 x 35 cm. The patient stands approximately 20 cm behind the polystyrene scattering panel which is mounted onto a platform 19 cm above the floor. The patient is rotated 120 degrees following each dual field thereby treating the anterior and both posterior oblique fields on one day and the posterior and both anterior oblique fields on the alternate day to comprise a two-day cycle of 12 exposures as described by Page et al. (1970). The term "dual field" refers to the treatment given by two broad electron beams in which the central axis of one beam is directed above the patient's head and the other is directed below the patient's feet. In the present 6-MeV technique, the gantry is angled 25 degrees below the horizontal and 17 degrees above the horizontal to comprise one dual field. Beam angulation in the dual field technique serves two purposes, namely to deliver a more uniform dosage to the patient than would be encountered with a horizontal field, and to place the forward peaked bremsstrahlung x-ray contamination of the electron beam outside the patient treatment volume (AAPM 1988; Karzmark 1964). Envelopes of TLD-100 powder are used to confirm patient dosage during the first treatment cycle and weekly throughout the treatment series as prescribed by a physician.

The objective of this research was to establish the 9-MeV dosimetric parameters for a total skin electron therapy technique on the Varian Clinac 18 at Mary Bird Perkins Cancer Center. The parameters have been determined using

both water and polystyrene phantoms. Calculated dosages were confirmed with the use of TLD-100 chips and powder envelopes on both a plywood panel erected in the treatment plane and on a cylindrical water phantom. The parameters required for boost fields that utilize high impact polystyrene scattering panels taped onto the distal apertures of the 6 x 6 cm, 10 x 10 cm, 15 x 15 cm, 20 x 20 cm, and the 25 x 25 cm electron cones for boost fields have been determined. Output determinations were made following the AAPM Task Group 21 protocol and stated in terms of cGy/monitor unit to permit the calculation of monitor units from prescribed dose.

MATERIALS AND METHODS

A. MATERIALS

1) Varian Clinac 18 Linear Accelerator

The Clinac 18 contains a standing wave accelerator structure that utilizes a klystron tube (Karzmark and Morton 1981). Beam capabilities include a 10 MV photon, and 6, 9, 12, 15, and 18 MeV electron beams. It is an isocentrically mounted machine having a 100 cm target-to-axis distance. The collimator jaws were opened to a 35 x 35 cm opening for all exposures when using the geometry of the total skin electron therapy technique. The output of the machine was calibrated using 400 MU per minute.

2) Polystyrene Scatterer/Degrader Panel and Platform

The polystyrene scattering panel (Figure 1) measures 100 x 212 x 0.635 cm and is vertically erected 9 cm from the front edge of a platform measuring 110 x 95 cm and 19 cm above the floor. The isocenter level is 111 cm above the platform and its position is 2 meters from the isocenter. Two wooden dowels are placed on the two shorter edges of the platform as patient supports. The platform is mounted on rollers for ease of mobility.

3) Plywood Panel (removable)

A removable 1.3 cm x 1 meter x 2 meter plywood panel was erected 20 cm behind the scattering panel. The function of the panel was to hold various dosimeters when investigating the optimal dual angle and dose uniformity in

FIGURE 1. Photograph of the polystyrene scattering/degrader panel placed at its routine treatment position.

the treatment plane. Kodak XV2 film was arranged in a grid fashion on the plywood to evaluate the horizontal and vertical uniformity of the beam and the relative dose existing in the treatment plane. TLD-100 chips were placed in locations most likely occupied by a patient.

4) Kodak XV2 Film

Calibrations using the nominal energies of 6 and 9 MeV electrons were made by placing 1- x 10-inch strips of film between the sections of a clear polystyrene phantom. The build-up thickness of polystyrene used was 1.07 cm and 1.6 cm for 6 and 9 MeV, respectively. Dutreix and Dutreix (1969) confirm the use of film as a valid relative dosimeter.

5) Kodak X-OMAT Automatic Processor

All films were developed in a Kodak X-OMAT film processor at a solution temperature of 35^0C. The background optical density was consistently 0.15.

6) Macbeth Transmission Densitometer TD-504 (#4489C)

The Macbeth TD-504 densitometer (Figure 2) provides a digital readout of optical density measurements from 0.0 to 4.0. The densitometer is equipped with a set of four color filters: red, blue, green, and gold. The blue filter was used.

7) Kodak Photographic Step Tablet No. 3 (#706ST121)

The photographic step tablet serves as an optical density reference when calibrating the Macbeth TD-504 densitometer. It contains 21 sections of

FIGURE 2. Photograph of the Macbeth TD-504 transmission densitometer and the photographic step tablet. The step tablet is the film strip lying horizontally in this picture.

diffuse densities ranging from 0.04 to 3.06. Particular attention was made to the range of optical densities encountered and the densitometer was calibrated for this range.

8) Phantoms

Different phantoms and dosimeters were used in an identical or a similar experiment for the purpose of corroborating results.

[a] Radiation Associates Scanner DPS (#820401) and Water Phantom

A major advantage of this system is its capacity for evaluting horizontal beams in a water medium. The water tank is equipped with a 2-mm end window. Attachments allow either a waterproofed Marcus parallel plate ionization chamber or a 0.6 cm^3 Farmer-type ionization chamber to be utilized. Since an insufficient signal was obtained with the Marcus chamber (PTW B23343, #291), a 0.6 cm^3 PTW 23333 (#1056) ionization chamber within a waterproof acrylic tube was used. The ionization chamber was connected to the modified Keithley 602 (#390556) electrometer. The scanner (Figure 3) permits movement in millimeter increments. Beam characteristics were evaluated 2 meters from the isocenter or at the location of the scattering panel and 20 cm behind the scattering panel. The water phantom proved to be easier to use than a polystyrene phantom, due to the manual shifting and accounting of individual polystyrene sections. However, a water phantom having a thin end window is required.

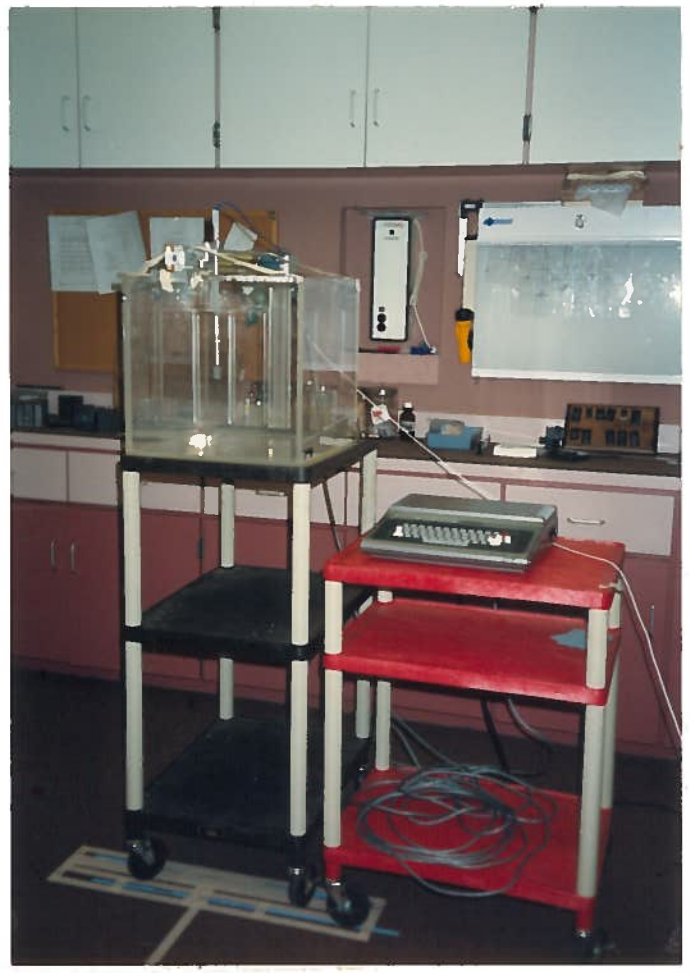

FIGURE 3. Photograph of the Radiation Associates scanner D.P.S. (#820401) and water phantom with 0.6 cm^3 PTW 23333 ionization chamber inside acrylic tube.

[b] Scrad Polystyrene Phantom

The Scrad polystyrene phantom contains 25 cm x 25 cm sections with 1.58, 12.7, 25.4, and 50.8 millimeter thicknesses held tightly in an acrylic frame. This acrylic frame also accommodates a Holt Memorial parallel plate ionization chamber (MPPK #233) (Figure 4). Beam characteristics were evaluated 2 meters from the isocenter and 20 cm behind the scattering panel.

[c] Nalgene Cylindrical Water Tank

A nalgene plastic water tank, 30 cm diameter, was used to evaluate the fractional contribution of one dual field with the use of film, ionization chamber, and TLD (Figure 5). An evaluation of the fractional contribution of each position around the tank was obtained. Although the use of a cylindrical polystyrene phantom was suggested in the A.A.P.M. Report #23 (1988), the nalgene tank was readily available. The thickness of the nalgene tank wall was 3 mm. The electron transmission through the nalgene wall using the nominal electron energy of 9 MeV was found to be 0.989.

[d] Med-Tech Water Phantom

Ionization profiles and calibrations were performed for a set of electron cones using the nominal energy of 9 MeV with the gantry in the beam down position exposing the water phantom from above. The sizes of the electron cones investigated are 6 x 6 cm^2, 10 x 10 cm^2, 15 x 15 cm^2, 20 x 20 cm^2, and 25 x 25 cm^2. Cone ratios and output factors were determined with and without high impact polystyrene scattering panels taped to the distal

FIGURE 4. Photograph of the Scrad polystyrene phantom with the Memorial parallel plate ionization chamber in its position 20 cm behind the scattering panel.

FIGURE 5. Photograph of the cylindrical nalgene water tank in position behind the scattering panel. Kodak XV2 film (black band) is arranged around the tank for the determination of the fractional contribution of a dual field.

apertures of each cone. Panels, 6.4-mm thick, were cut specifically for each cone. The panel size corresponding to the above cones are 12.3 x 12.3 cm^2, 16 x 16 cm^2, 21.3 x 21.3 cm^2, 25.5 x 25.5 cm^2, and 30 x 30 cm^2. Also, beam characteristics for the 25 x 25 cm^2 cone with an 0.5 cm acrylic panel attached were obtained. A waterproof PTW 233641 (#693) was connected to the Keithley 614 electrometer (#330327). This technique of treatment using a scattering panel taped to the electron cone aperture is for boosting areas of the body that have received less than the prescribed dose after using the six dual field technique.

[e] Wax-Water Phantom

Two thin walled ($\leq$ 1mm) plastic near-cylindrical containers were obtained and modified for the purpose of estimating the depth of maximum dose when curved surfaces are exposed during the 9 MeV six dual field technique. The phantom is shown in Figure 6 with the bottoms of the containers placed together sandwiching a circular piece of XV2 film between them and positioned so that the plane of the film is horizontal and at the same height as the isocenter. The container above the film is filled with water to the level of 10 cm while the container below contains 5 cm of wax adjacent to its bottom. Since the practical range of electrons was shown to be less than 4 cm, the thicknesses of water and wax sandwiching the film is sufficient for producing a realistic scatter component of dose. A horizontal layer of wax was added to the outside bottom surfaces of the containers to permit a flat surface

FIGURE 6. Photograph of the wax-water phantom in position 20 cm behind the scattering panel. The two containers are set with their bottoms together sandwiching a circular piece of film. The upper container contains water and the lower, inverted contains wax against its bottom.

against the film. The film was carefully cut from a larger piece of film and placed between the containers to eliminate the maximum amount of air from the surface of the film and to prevent any portion of the film from projecting beyond the circular bottoms of the containers. The phantom was positioned and exposed to the six dual fields with a 60-degree rotation of the phantom made after each dual field.

9) Thermoluminescent Dosimeters (LiF)

[a] TLD Powder

Lithium fluoride powder in small envelopes were obtained from a supplier in Houston, Texas. Experiments were performed to confirm the delivery of a prescribed dose of 100 cGy based upon the results obtained from XV2 film, to obtain the fractional contribution for a dual field and the contribution of one dual field to each position around the nalgene water tank.

[b] TLD-100 Chips

TLD-100 chips (LiF) were used to confirm the dosage in an area of the treatment plane which would most likely be occupied by a patient. These locations and results are illustrated in Figure 22 of the next section. One-hundred twenty-five (125) TLD-100 chips measuring 0.125 x 0.125 x 0.035 inches were obtained from Engelhard-Harshaw Company. The responses in microcoulombs were obtained from Radiation Late Effects, M.D. Anderson Hosptial, Houston, Texas, from which 43 chips were selected for use. Calibrations and sensitivity experiments were performed with the chips inside

a clear polystyrene irradiation phantom. The phantom measures 1 x 25 x 25 cm and contains a 0.73 mm middle section which the chips occupy, and a 6.73-mm upper section. The response curves of 125 thermoluminescent dosimeter chips (TLD-100) were evaluated from which 43 chips were selected for use as dosimeters. The response of a chip near the center of the irradiation phantom was selected for the normalization of all TLD response values. All TLD response values were normalized to this reading and labeled as the sensitivity for the individual chip. The response from an exposure was then multiplied by the sensitivity of the chip to obtain a corrected reading before determining the dose from the calibration curve. All handling of the chips was made using vacuum tweezers. The chips were sealed into small plastic bags and labeled before their placement onto the plywood panel when confirming dosage to the treatment plane.

10) Victoreen Annealing Oven Model 2600-62 (#1184)

The TLD-100 chips were annealed at 400^0C for one hour followed by 80^0C for 24 hours as prescribed by Zimmerman et al. (1966). The chips were annealed in a cured aluminum TLD planchet.

11) Mannequin

A mannequin composed of fiberglass and metal joints was obtained from a local department store in an effort to simulate a patient undergoing the total skin electron therapeutic technique. TLD chips and powder envelopes were placed on the mannequin at various locations and doses were delivered using

both 6 and 9 MeV electrons with the six dual field technique. The mannequin was irradiated in the same fashion as a patient receiving a 200 cGy treatment.

B. METHODS

1) Output Stability Check

All measurements and experiments for this study were performed on the Varian Clinac 18 except for the measurements required for the N_{gas} calculation of the Holt Memorial parallel plate chamber which were done on the Varian Clinac 20. Output constancy checks on the Clinac 18 were performed before and after all experiments. The average of three readings obtained with a Keithley 614 (#330327) electrometer and PTW N23333 (#290) Farmer-type ionization chamber, the system routinely employed for constancy checks on the Clinac 18, was multiplied by a temperature-atmospheric pressure correction factor. A ratio of this value to the expected value constitutes the constancy check. The output was adjusted if the constancy value was greater than $\pm 2\%$. The temperature-atmospheric pressure correction (TPC) was obtained using the following equation:

$$TPC = \frac{T+273.15}{295.15} \times \frac{760}{P}$$

where T is the temperature in degrees centigrade and P is the atmospheric pressure in mmHg. All exposures were made with the nominal electron energies of 6 and 9 MeV.

2) Energy and Dose Determination

The energy and dose determinations made in this study follow those recommended by the AAPM TG-21 protocol (AAPM 1983). The mean electron energy $(\bar{E}_0)$ at the phantom surface is proportional to the depth at half of the maximum ionization (d_{50}) in water:

$$\bar{E}_0 = 2.33 \left(\frac{MeV}{cm}\right) * d_{50}(cm) .$$

The scaling factor used for polystyrene is 0.965 (cm of water/cm of polystyrene). The mean electron energy at the depth of measurement $(\bar{E}_z)$ is directly related to the depth of measurement (Z) and inversely related to the practical range (Rp):

$$\bar{E}_z = \bar{E}_0 \left(1 - \frac{Z}{R_p}\right).$$

The mean electron energy at the phantom surface and the mean electron energy at depth are the only parameters of energy determined in this study because of their requirement in dosimetric calculations. The values of the depth of maximum dose (d_{max}), d_{50} and Rp in each experiment were obtained from the relative ionization versus depth curve generated from the data. The practical range is determined at the point of intersection of the line extending along the lower, decreasing one-third of the curve and the line representing the bremsstrahlung background referred to as the x-ray contamination (Loevinger et al. 1961). The depth of maximum ionization is represented by the highest point on the curve.

An N_{gas} value, the cavity-gas calibration factor, was required for the cylindrical Farmer-type ionization chamber PTW N23333 (#768) and was obtained as recommended by the AAPM (1983):

$$N_{gas} = \frac{k(W/e)\, A_{ion}\, A_{wall}\, \beta}{\alpha \left(\frac{\bar{L}}{\rho}\right)_{air}^{wall} \left(\frac{\bar{\mu}_{en}}{\rho}\right)_{wall}^{air} + (1-\alpha) \left(\frac{\bar{L}}{\rho}\right)_{air}^{cap} \left(\frac{\bar{\mu}_{en}}{\rho}\right)_{cap}^{air}}$$

where N_x is the exposure calibration factor (R/C), k is the charge produced in air per unit mass per unit exposure, 2.58 x 10^{-4} C/kg•R, W/e is the mean energy expended per unit charge in air, 33.7 J/C, and A_{ion} is the ion-collection efficiency of the chamber at the time of calibration. A_{wall} is the correction factor for attenuation and scatter in the wall and build-up cap. Beta (ß) is the ratio of the absorbed dose to the collision fraction of kerma, 1.005. Alpha (α) is the fraction of ionization related to electrons from the chamber wall. $\left(\frac{\bar{L}}{\rho}\right)_{air}^{wall}$ is the ratio of the mean restricted collision mass stopping power of the wall material to that of air, and $\left(\frac{\bar{L}}{\rho}\right)_{air}^{cap}$ is the ratio of the mean restricted collision mass stopping power of the build-up cap material to that of air. $\left(\frac{\bar{\mu}_{en}}{\rho}\right)_{wall}^{air}$ is the ratio of the mean mass energy absorption coefficient of air to that of wall material, and $\left(\frac{\bar{\mu}_{en}}{\rho}\right)_{cap}^{air}$ is the ratio of the mean mass energy absorption coefficient of the air to that of the build-up cap material. The N_{gas} value for the PTW N23333 #768 is 4.69 x 10^7 Gy/C.

An N_{gas} determination was required for the Holt Memorial Parallel Plate ionization chamber (MPPK 233). The method of determination followed the

AAPM (1983) recommendation by comparing the parallel plate (P-P) chamber to a calibrated cylindrical chamber (Cyl):

$$(N_{gas})^{P-P} = \frac{(M\ N_{gas}\ P_{ion}\ P_{repl})}{(M\ P_{ion})}$$

where M is the electrometer reading in coulombs, N_{gas} is the cavity-gas calibration factor in cGy/coulomb, P_{ion} is the ion recombination correction factor, and P_{repl} is the electron fluence replacement factor. P_{repl} for the Holt Memorial chamber is considered 1.00 (Holt et al. 1979). The N_{gas} value for this Holt Memorial parallel plate chamber was calculated to be 2.4×10^7 Gy/C.

Output determinations were obtained in terms of dose to muscle (cGy/monitor unit):

$$\dot{D} = \frac{M}{MU+e} * TPC * ECF * \left(\frac{\bar{L}}{\rho}\right)_{air}^{water} * P_{ion} * P_{repl} * \left(\frac{\bar{S}}{\rho}\right)_{water}^{muscle} * N_x * \frac{N_{gas}}{N_x} A_{ion}$$

where $\dot{D}$ is the dose rate in cGy/MU, (MU+e) is the sum of monitor units used and the timing error, ECF is the electrometer correction factor, $\left(\frac{\bar{L}}{\rho}\right)_{air}^{water}$ is the ratio of the mean restricted collision stopping power of water to that of air, and $\left(\frac{\bar{S}}{\rho}\right)_{water}^{muscle}$ is the ratio of the mean unrestricted collision mass stopping power of muscle to that of water. The ratio of the mean unrestricted collision mass stopping power of water to that of polystyrene $\left(\frac{\bar{S}}{\rho}\right)_{poly}^{water}$, and the ratio of the electron fluence in water to that of polystyrene ϕ_{poly}^{water} were additional factors used whenever polystyrene phantoms were used.

3) Calculation of Monitor Units

The formula adopted for calculating the number of monitor units required to deliver a specified dose is:

$$\text{MU/Field} = \frac{\text{Prescribed dose x fractional contribution per d.f.}}{2 \text{ x output per d.f.}}$$

This formula is a modification of the one given in the AAPM Report #23 (1988). The Report applies a factor called "B" to account for overlapping fields. The fractional contribution of a dual field in this paper is the reciprocal of this "B" factor and is further discussed in the **Results and Discussion** section under *Single Dual Field Fractional Contribution.*

One should infer that MU/field refers to the setting for one of twelve exposures to be made in one cycle. (The symbol, "d.f.", refers to dual field.) The fractional contribution per dual field was obtained by dividing the dose from one dual field by the mean dose obtained from six locations of the same height at 60-degree increments around a cylindrical water phantom after its positioning and exposure to all six dual fields.

4) Experimental Set-up

Knowledge of the treatment room dimensions are essential to the design of a total skin electron therapy technique that utilizes target-to-skin distances in the range of 3 meters. The apparatus containing the polystyrene panel and the distance required to design a vertically uniform dual field must fit into the size of the room.

The six dual field technique incorporates two angles, one above and the other below the horizontal, to uniformly distribute the dose to the patient. The projection of the isocenter horizontally to and beyond the scattering panel onto the treatment plane provides reference points in the plane of the scattering panel and in the treatment plane. The reference point located on the scattering panel will be referred to as the "isocenter level" while the reference point located in the treatment plane along the horizontal beyond the scatterer is referred to as the calibration point. The treatment plane in this study is a plane located 20 cm behind the scattering panel and perpendicular to a horizontal ray as recommended by the AAPM Report #23 (1988). This plane is examined when making determinations of interest to patient dosimetry. To assure reproducibility of set-up, the vertical distances above and below the isocenter level were calculated for each dual angle to be investigated and marked on the polystyrene panel (Table 1). Figures 7 and 8 illustrate the geometries used in this study. Measurements made with each geometry provide important comparisons in beam parameters. Figure 7 illustrates measurements made with horizontal beams with and without the insertion of a scatterer. Figure 8 illustrates the geometry used in evaluating a dual angle.

The location of the isocenter was determined by centering on a pointer with the gantry first in the vertical position, then rotating the gantry to the horizontal position, and raising the pointer until it intersects the central axis of the horizontal beam. A plumb bob was hung from the isocenter to the floor.

TABLE 1

The distances above and below the isocenter level marked on the polystyrene scattering panel for each dual angle investigated.

Dual Angle	Distance From the Isocenter Level (cm)*
17^0	61.1
18^0	65.0
19^0	68.9
19.6^0	71.2
20^0	72.8
21^0	76.8

*vertical distance = 200 tan θ

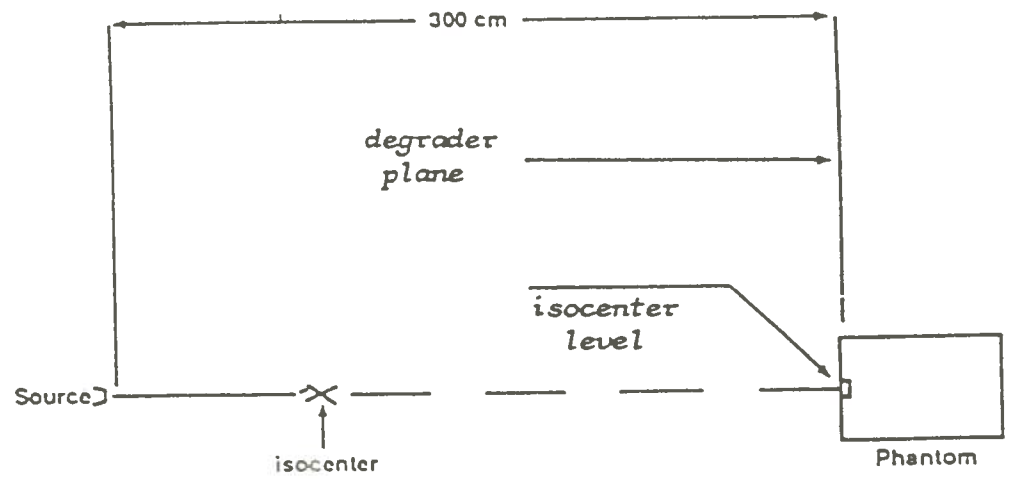

a.

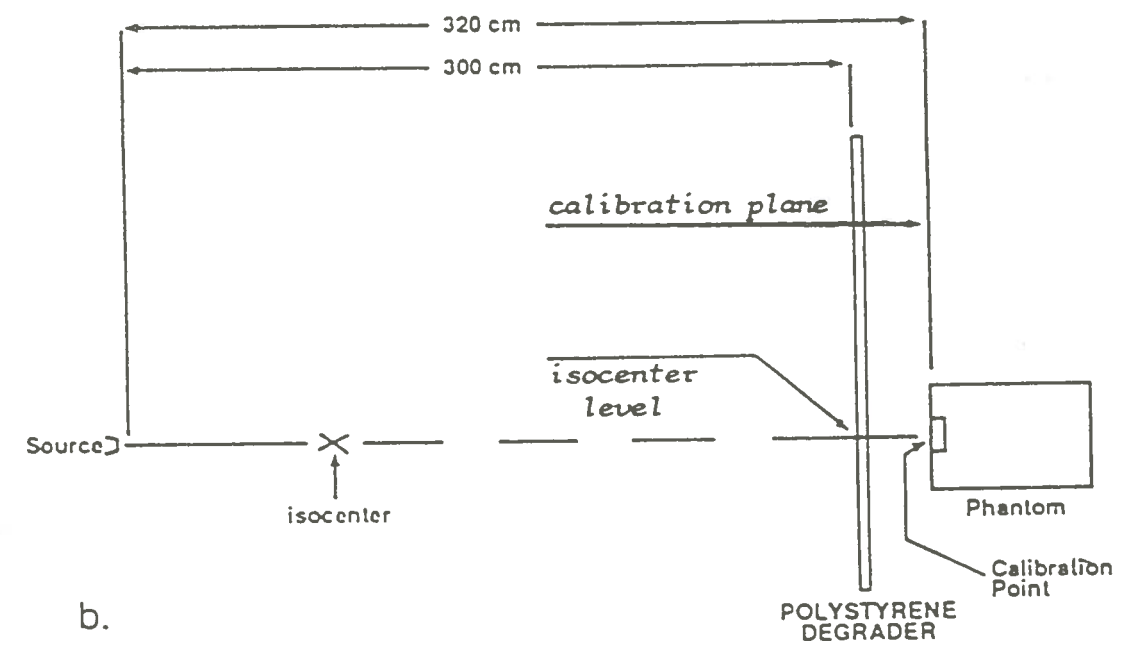

b.

FIGURE 7. Diagram of the geometry of measurements involving the horizontal beam. **a.** The phantom is placed in the same position as the scattering panel surface to measure beam characteristics at 300 cm SSD. **b.** The phantom is then placed 20 cm behind the scattering panel, the location of the treatment plane to measure beam characteristics after the insertion of the scatterer into the beam at 300 cm from the source.

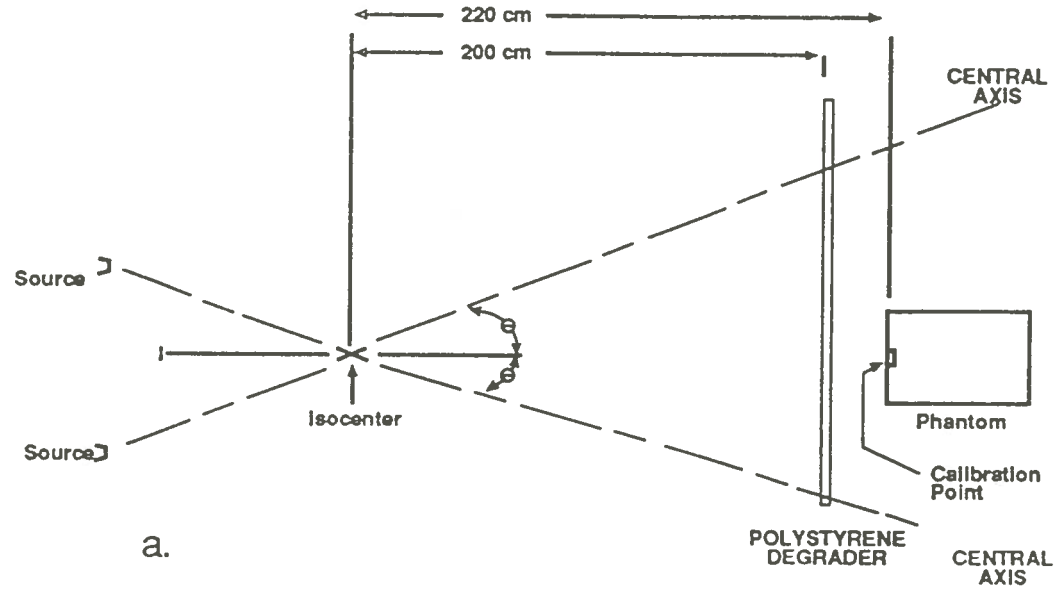

FIGURE 8. Diagram of the geometry of measurements involving the beams of a dual angle. **a.** The placement of the phantom in the treatment plane. **b.** The plywood panel occupies the whole treatment plane and functions as a surface for the attachment of various dosimeters for measurements in the treatment plane.

After repeated placements of a plumb bob and acceptable collimator rotation tests with the gantry in the beam-down position, there was a 4-mm maximum difference in distance between the point obtained by projecting the crosshair onto the floor and the points obtained from repeated suspensions of the plumb bob. The path followed as the shadow of the crosshair travels on the floor when the gantry is rotated provides a line of measurement from the isocenter. Two points were made on this line at 191 cm and 200 cm from the vertical projection of the isocenter. Perpendicular lines were drawn through these two points. The line at 191 cm was made for aligning the front edge of the platform containing the scattering panel which is 9 cm from the edge of the platform. The line at the 200 cm distance was drawn for experiments evaluating the beam at the surface of the scatterer.

5) Dual Angle Determination

[a] Survey with Ionization Chambers

A survey of various dual angles were made by taping two ionization chambers with their buildup caps to the plywood panel with one at the calibration point and the other at the intersection of the central ray on the scattering panel for each angle investigated. The PTW 23333 (#768) ionization chamber was fixed to the calibration point and connected to the modified Keithley 602 (#390556) electrometer via a triaxial cable. The PTW 23333 (#290) ionization chamber was taped to the plywood at a height corresponding to the dual angle to be investigated and connected to the

Keithley 614 (#330327) electrometer via a triaxial cable. The dual angles surveyed varied from 14 to 24 degrees. The design of the survey was such that the optimal angle would result in a value equal to twice the value measured at the calibration point. The value expected at the calibration point was subtracted from the measured value. The average value observed on the electrometers was multiplied by the electrometer correction factor (ECF) and the N_x value of the chamber obtained from the calibration lab. Kumar et al. (1977) and Edelstein et al. used this design by matching together two 50% isodose lines from separate exposures to create a dual angle.

[b] Determination with Kodak XV2 Film

Film strips were placed in a vertical arrangement in the center of the plywood facing the scattering panel and exposed to one dual field. This was repeated for each dual angle investigated. The dual angle providing the least optical density variation was regarded as the one giving the best uniformity in the treatment plane. The film strip arrangement used to evaluate the vertical uniformity is illustrated in Figure 9.

6) Film Dosimetry

[a] Relative Dose in the Treatment Plane

Once the dual angle providing the best vertical uniformity was selected, film strips were placed in a grid fashion on the plywood (Figure 10) to evalute the relative dose distribution throughout the treatment plane.

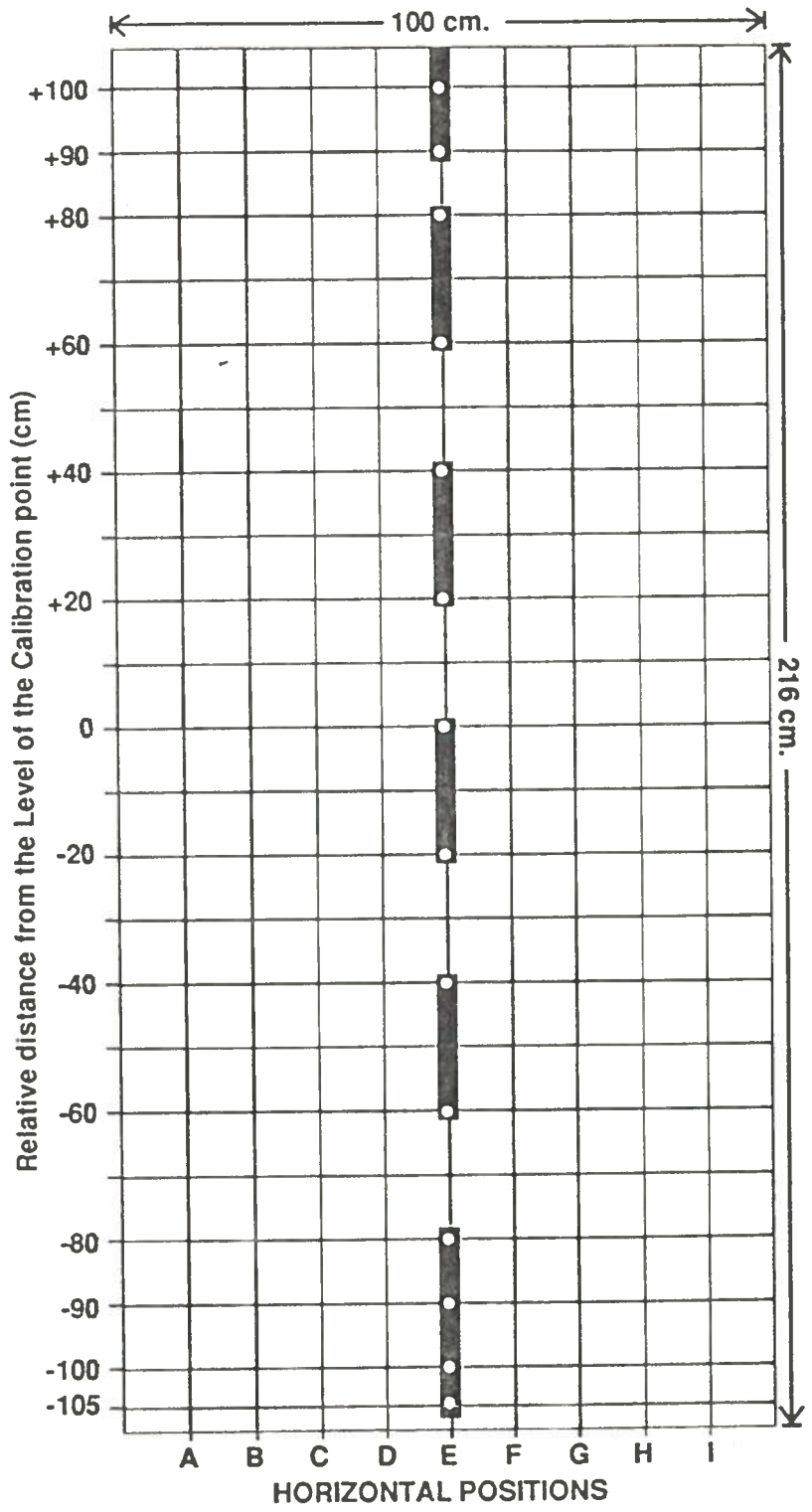

FIGURE 9. Diagram of the placement of XV2 film strips on a plywood panel erected in the treatment plane for the evaluation of the vertical uniformity in dose of each dual angle investigated.

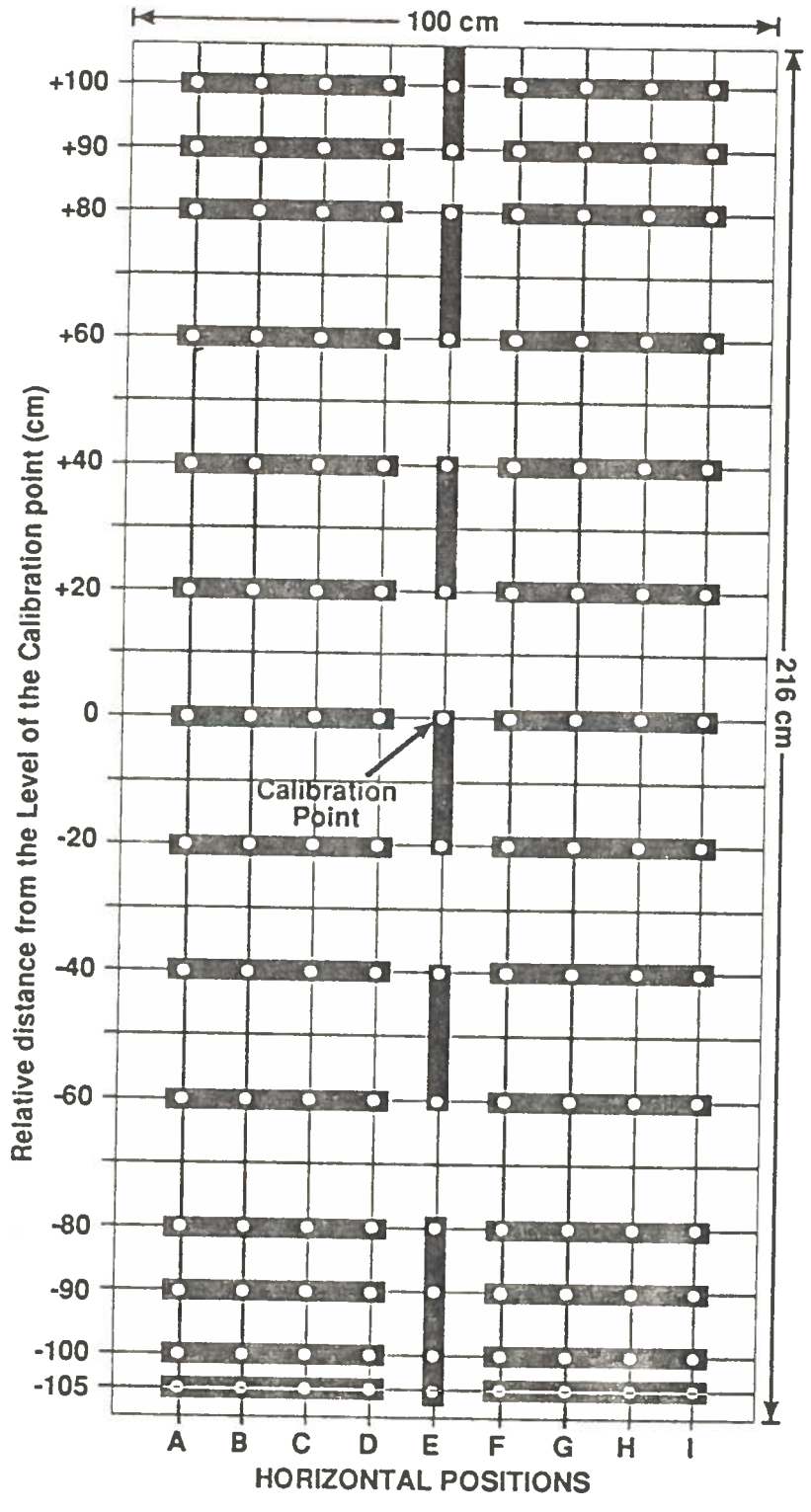

FIGURE 10. Diagram of the placement of XV2 film strips on a plywood panel erected in the treatment plane for relative dose evaluation.

[b] Determination of the Fractional Contribution of a Dual Field

Film strips were used to determine the fractional contribution of one dual field. Film strips, 1 x 10 inches, were wrapped around a water filled nalgene plastic tank at the level of the calibration point (Figure 5). Because exposure to the patient is distributed around the patient in 60-degree increments (seen later in Figure 21), the simulation of these positions was made by rotating the cylindrical water tank in 60-degree increments after irradiation of each dual angle. The tank was positioned in the center of the treatment plane with the closest surface 20 cm behind the scattering panel. As a result, the tank was exposed at six different positions which are illustrated in Figure 11. (Figure 11 illustrates TLD placement but the positions of measurement with film are the same.)

[c] Determination of the d_{max} value on a Cylindrical Phantom (Wax-Water Phantom)

Circular cutouts of film having the same diameter as the wax-water phantom (25.5 cm diameter) were used to evaluate how a curved surface affects the depth dose of electrons. The placement of the film is described in the *Wax-Water Phantom* section.

6) TLD Dosimetry (LiF)

[a] Determination of the Fractional Contribution of a Dual Field

Six TLD powder envelopes were placed around the nalgene water tank at 60-degree increments at the height of the calibration point. The tank

was then oriented so that one of the TLDs was at a point closest to the direction of the beam. The tank was rotated 60 degrees after the irradiation of each dual field. Twelve irradiations constitute a complete treatment cycle. This experiment served to confirm the delivery of a prescribed dose of 100 cGy using the beam parameters and information obtained from film.

The number of monitor units to deliver 100 cGy was calculated based upon the fractional contribution obtained with film (0.3515 given in Table 7) and the output obtained using the Holt Memorial Parallel Plate chamber (0.0366 cGy/MU given in Table 6). Figure 11 shows the placement scheme of the TLD powder envelopes. The tank was filled with water and exposed using the six dual field technique ($+19^0/-19.6^0$) and 960 MU/d.f. Three controls were used in calibrating the dose received by the TLDs.

[b] Determination of the Contribution of One Dual Field to Each Position Around a Cylindrical Phantom

Powder envelopes were placed on the nalgene tank at the locations specified in Figure 11 with one TLD (labeled #1) remaining on the tank throughout the six dual field cycle and the others (labeled a – f) being replaced after every dual field. Three TLD envelopes were used as controls for TLD calibration.

[c] Relative Dose in the Treatment Plane

TLD-100 chips were used to evaluate the relative dose in the treatment plane at locations most likely occupied by a patient. These locations

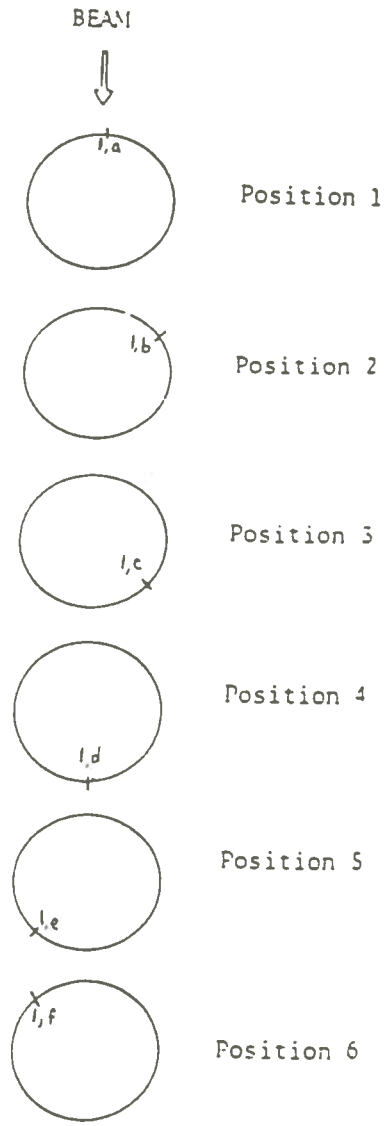

FIGURE 11. The placement scheme of TLD-100 powder envelopes onto the surface of the cylindrical water tank to determine the contribution at each location and the fractional contribution of a dual field. When determining the contribution at each location, TLD #1 remains on the tank throughout the complete cycle while TLDs a–f are replaced after each 60-degree rotation. The tick marks on the circumference of the phantom illustrate the original location relative to the direction of the beam after each 60-degree rotation. When determining the fractional contribution of a dual field, six TLDs are placed on the phantom and remain throughout the complete cycle of treatment.

and results are illustrated in Figure 22 of the *Results and Discussion* section.

8) Ionization Chamber Dosimetry

[a] Determination of Beam Parameters

Depth profile measurements were obtained using water phantoms and a clear polystyrene (Scrad) phantom. Beam parameters were generated for the geometries given in Figures 7 and 8 using a polystyrene phantom. Depth profile measurements were generated for the various electron cones using the Med-Tech water phantom.

[b] Determination of the Contribution of One Dual Field to Each Position Around a Cylindrical Phantom

A waterproof PTW 233641 (#693) 0.3 cm^3 ionization chamber was fixed to the inside wall of the nalgene tank at the effective depth which included the nalgene thickness of 0.8 cm, and connected to the modified Keithley 602 (#390556) electrometer via a triaxial cable. Six $+19^0/-19.6^0$ dual field irradiations (800 MU/d.f.) were given with the tank being turned 60 degrees between each dual field to each position in the same fashion as illustrated on Figure 11. (Figure 11 refers to TLD placement but orientation of the positions for the ionization chamber are the same.)

RESULTS AND DISCUSSION

This study of the 9 MeV total skin electron therapy technique was based upon four goals: (1) the determination of the dual angle providing the most vertically uniform dose; (2) the determination of beam characteristics and output in the plane of the scattering panel, in the treatment plane, and when utilizing the electron cones at a distance of 100 cm; (3) the determination of factors accounting for the contribution of each dual field to the total dose delivered and relating monitor units to prescribed dose using these factors; and (4) the confirmation of the dose delivered based upon the dose prescribed. Results are based upon ionization chamber data and corroborated by Kodak XV2 film and TLD dosimetry or through the use of different phantoms.

A. Dual Angle Determination

The initial survey conducted using ionization chambers taped onto the plywood panel fixed at the treatment plane resulted in the 20-degree gantry angle arrangement giving the least difference betwen the measured and expected values at the calibration point. Table 2 gives the results of all the angles investigated in the initial survey.

Kodak XV2 film was placed in the center vertical axis of the plywood panel as shown in Figure 7 for each dual angle investigated. Dual angles ±17, ±18, ±19, ±20, and ±21 degrees were investigated. (The + and – indicate the gantry angle projecting above and below the horizontal, respectively.) Table 3 displays optical

TABLE 2

Example of single angle survey with ionization chambers taped to the plywood showing the 20^0 angle to be the best angle by providing the least difference between the measured and expected readings. The table shows only the angle pointing up.

Single angle surveyed	Gantry angle used*	Distance of CAX above isocenter level (cm)	M** on CAX	M** at calibration point	Expected*** M at calibration point	Difference
24	294	89.0	16.175	4.010	8.087	-4.077
23	293	84.9	16.300	5.180	8.150	-2.970
22	292	80.0	16.551	6.127	8.276	-2.149
21	291	76.8	16.712	7.519	8.356	-0.837
20	290	72.8	16.891	8.447	8.446	0.001
19	289	68.9	17.053	9.468	8.526	0.942
18	288	65.0	17.196	10.861	8.598	2.263
17	287	61.1	17.321	11.789	8.661	3.128
16	286	57.3	17.429	13.033	8.715	4.319
15	285	53.6	17.590	13.720	8.795	4.925

*Gantry angle 270^0 provides a horizontal beam

**M = electrometer reading x electrometer correction factor x N_x of the appropriate chamber

***The term "expected" denotes that value received at the calibration point that would result in the next optimum dual angle. The smallest difference between expected and measured values specifies the dual angle most likely to deliver the most vertically uniform dose.

TABLE 3

Optical densities from XV2 film for comparing vertical uniformity in exposure for each dual angle.

DUAL ANGLE	17°		18°		19°		20°		21°	
Distance (cm) from cal. point	OD	N*	OD	N*	OD	N*	OD	N*	OD	N**
+100	0.55	0.866	0.57	1.102	0.57	0.912	0.57	0.927	0.58	0.935
+90	0.59	0.929	0.60	0.945	0.60	0.960	0.60	0.976	0.60	0.968
+80	0.62	0.976	0.62	0.976	0.62	0.992	0.61	0.992	0.62	1.000
+60	0.63	0.992	0.62	0.976	0.62	0.992	0.62	1.008	0.61	0.984
+40	0.67	1.055	0.64	1.008	0.62	0.992	0.60	0.976	0.59	0.952
+20	0.71	1.118	0.66	1.039	0.62	0.992	0.58	0.943	0.53	0.855
0	0.77	1.213	0.68	1.071	0.62	0.992	0.55	0.894	0.49	0.790
-20	0.72	1.134	0.68	1.071	0.62	0.992	0.58	0.943	0.51	0.823
-40	0.68	1.071	0.66	1.039	0.65	1.040	0.62	1.008	0.59	0.952
-60	0.64	1.008	0.65	1.024	0.63	1.008	0.62	1.008	0.62	1.000
-80	0.61	0.961	0.62	0.976	0.63	1.008	0.62	1.008	0.62	1.000
-90	0.60	0.945	0.61	0.961	0.63	1.008	0.61	0.992	0.61	0.984
-100	0.57	0.898	0.59	0.929	0.61	0.976	0.60	0.976	0.61	0.984
-105	0.58	0.913	0.59	0.929	0.61	0.976	0.60	0.976	0.61	0.984

OD = optical density

N* = normalization to the average of the +60 and -60 values

N** = normalization to the average of the +80 and -80 values.

For each dual angle investigated, normalizations were made at the point located closest to the intersection of the central ray and the polystyrene panel.

densities obtained after a 300 monitor unit exposure to each field comprising one dual field (600 MU per dual field). Figure 12 is a graphic presentation of the data in Table 3 which shows a sharp increase in optical density of 0.65 which is 4% above the normalized value of 0.625 at the −40 cm level on the curve representing the ±19 degree dual angle. In an effort to reduce this sharp increase and give a more uniform exposure, the ±19.6 degree dual angle was investigated along with the unequal dual angle +19 degrees and −19.6 degrees (designated hereafter as $+19^0/-19.6^0$). The $\pm 19^0$ dual angle was repeated and included in Figure 13 and also in Table 4. The difference between the value of 1.00 at the calibration point and the normalized value at each height in the plane of calibration were totalled for each angle investigated. The unequal dual angle $+19^0/-19.6^0$ shows the least total deviation from the normalized value and was therefore selected as the dual angle producing the most vertically uniform dose. This dual angle was used throughout the rest of the project. These angles are reproducible because points were marked on the scattering panel at the distances corresponding to each gantry angle used (Table 1). Reproducibility is acceptable so long as the scattering panel is accurately positioned at the assigned distance from the source.

B. Relative Dose in the Treatment Plane

Optical densities were measured using 34 strips of XV2 film arranged as shown in Figure 10. The $+19^0/-19.6^0$ dual angle was used with 300 MU per exposure. A tabulation of the optical densities at each point of measurement on the plywood is given in Table 5. The optical densities obtained in the treatment plane in the area

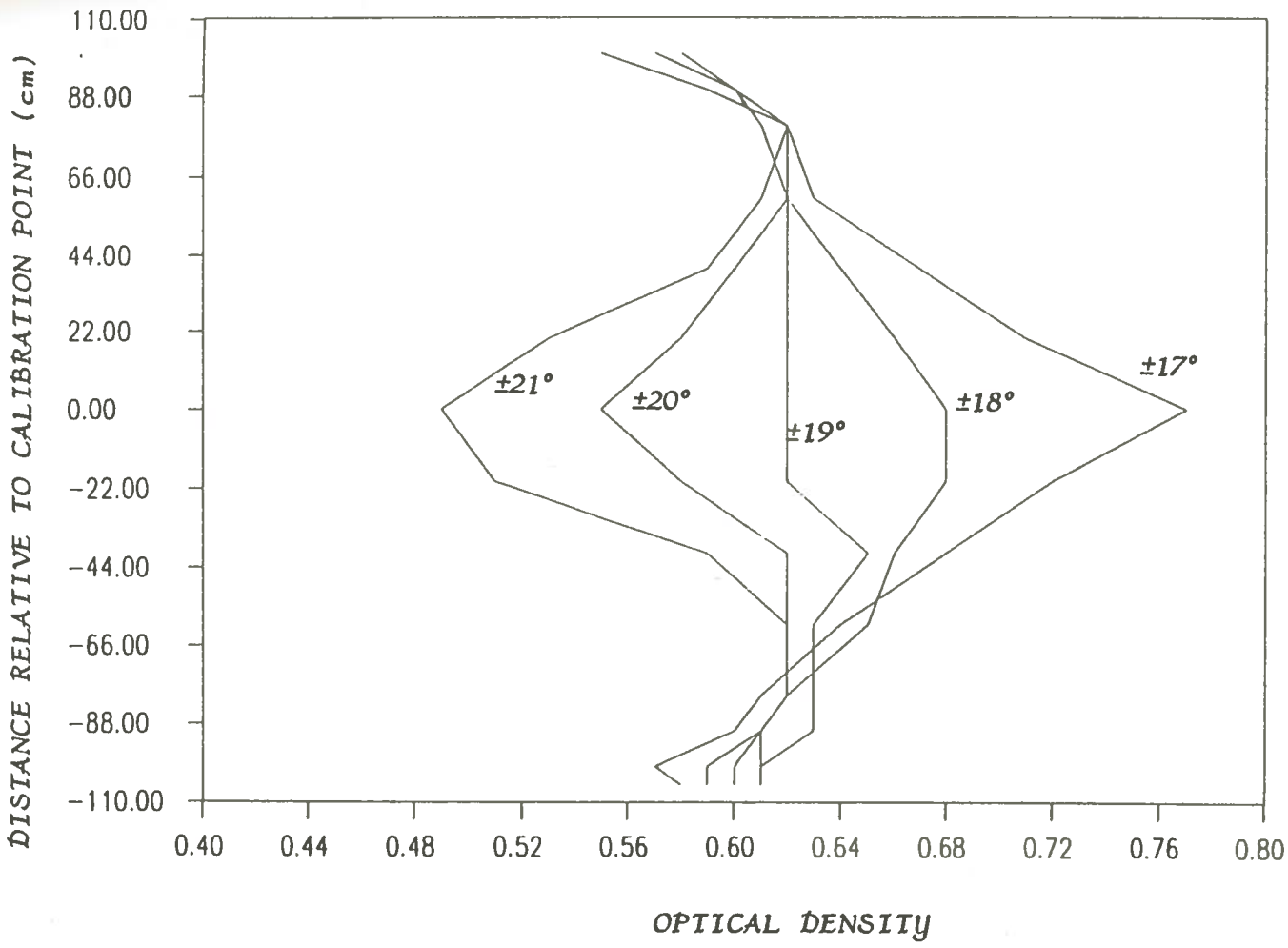

FIGURE 12. Graphic presentation of the data of Table 4 showing the greatest vertical uniformity of the five dual angles investigated being produced with the ±19 angle.

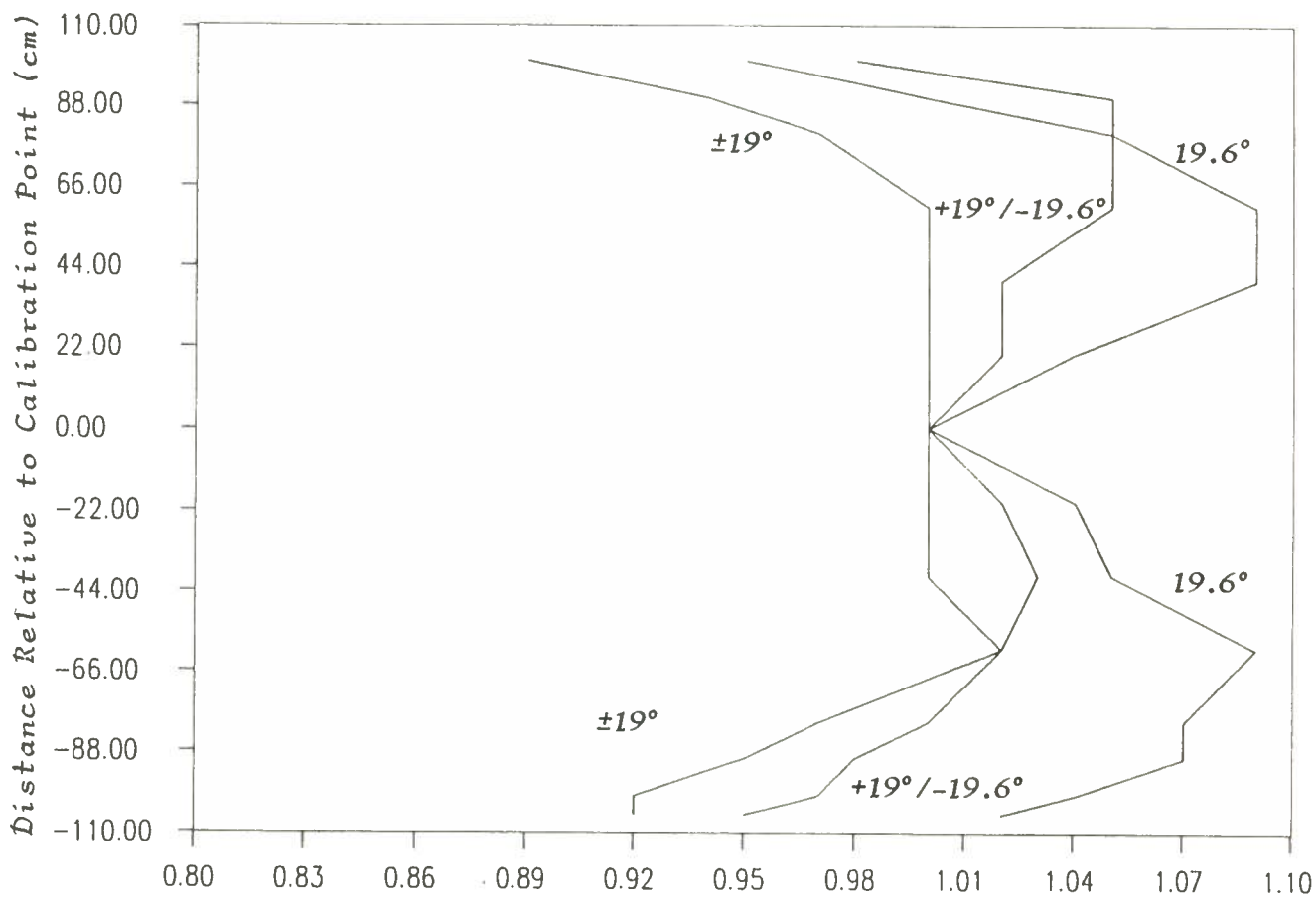

FIGURE 13. Graphic presentation of Table 5. The unequal dual angle of $+19^0/-19.6^0$ produces the least total deviation from the normalized value which was made at the calibration point.

TABLE 4

Optical densities from XV2 film for comparing vertical uniformity in exposure for $\pm 19^0$, $+19/-19.6^0$ and $\pm 19.6^0$ dual angles.

DUAL ANGLE

Distance relative to cal. point (cm)	±19°		+19°/−19.6°		+19.6°	
	OD	N*	OD	N*	OD	N*
+100	0.55	0.89	0.56	0.95	0.56	0.98
+90	0.58	0.94	0.59	1.00	0.60	1.05
+80	0.60	0.97	0.62	1.05	0.60	1.05
+60	0.62	1.00	0.62	1.05	0.62	1.09
+40	0.62	1.00	0.60	1.02	0.62	1.09
+20	0.62	1.00	0.60	1.02	0.59	1.04
0	0.62	1.00	0.59	1.00	0.57	1.00
-20	0.62	1.00	0.60	1.02	0.59	1.04
-40	0.62	1.00	0.61	1.03	0.60	1.05
-60	0.63	1.02	0.60	1.02	0.62	1.09
-80	0.60	0.97	0.59	1.00	0.61	1.07
-90	0.59	0.95	0.58	0.98	0.61	1.07
-100	0.57	0.92	0.57	0.97	0.59	1.04
-105	0.57	0.92	0.56	0.95	0.58	1.02

OD = optical density

N^* = normalization was made to the value obtained at the calibration point (0.00 cm) for each dual angle.

TABLE 5

Tabulation of optical densities obtained in the treatment plane using the $+19/-19.6^0$ and dual angle. Each horizontal position is 10 cm apart. Position E at 0 cm relative distance refers to the calibration point (600 MU/dual field).

Distance Relative to the Calibration Point	HORIZONTAL POSITIONS								
	A	B	C	D	E	F	G	H	I
+100	0.50	0.50	0.53	0.56	0.56	0.58	0.55	0.55	0.57
+ 90	0.53	0.54	0.56	0.59	0.59	0.59	0.57	0.55	0.54
+ 80	0.54	0.55	0.57	0.60	0.60	0.60	0.57	0.56	0.55
+ 60	0.56	0.56	0.58	0.61	0.60	0.62	0.60	0.58	0.58
+ 40	0.55	0.56	0.58	0.60	0.60	0.60	0.59	0.60	0.56
+ 20	0.54	0.57	0.58	0.62	0.60	0.59	0.58	0.56	0.56
0	0.52	0.54	0.56	0.59	0.59	0.58	0.57	0.55	0.55
- 20	0.53	0.55	0.56	0.59	0.59	0.60	0.58	0.56	0.57
- 40	0.56	0.56	0.58	0.60	0.61	0.62	0.60	0.58	0.57
- 60	0.57	0.56	0.58	0.60	0.61	0.63	0.61	0.59	0.60
- 80	0.57	0.56	0.58	0.60	0.60	0.60	0.58	0.58	0.56
- 90	0.55	0.55	0.57	0.60	0.59	0.60	0.59	0.58	0.60
-100	0.54	0.53	0.55	0.58	0.58	0.58	0.56	0.56	0.57
-105	0.56	0.53	0.56	0.59	0.58	0.60	0.57	0.56	0.56

most likely occupied by a patient as illustrated in Figure 22 for TLD chips, result in a standard deviation of 4.3% of the mean value. These optical densities of Table 5 were normalized to demonstrate vertical and horizontal variations. Horizontal variations are displayed with each horizontal row normalized to the value in Column E, the horizontally central position on the plywood. Vertical variations are displayed with each vertical column normalized to the value at the level of the calibration point. Figure 14 shows a greater horizontal variation on the left side with the average normalized value of 0.92 in Column A. Greater vertical variation occurs at the periphery of the field with greater uniformity toward the central portions (Figure 15). Columns A, H, and I of Figure 15 have average normalized values of 1.049, 1.033, and 1.032, respectively, whereas the centrally located Columns B, C, D, E, and G have average normalized values of 1.015, 1.015, 1.009, 1.005, and 1.018. Although Column F is centrally located and has an average normalized value of 1.032, central vertical uniformity is still the general pattern of optical density.

The plane of investigation in this study is 20 centimeters wider and 5 centimeters longer than the one given in a similar study in the AAPM Report #23. This study contains 47 points more than the one in the AAPM Report #23. If the values given in the Report are normalized and evaluated in the same fashion as this study, a comparison of the same points reveals that the highest average of normalized values for a column or row is 1.031 which is calculated for the vertical column represented as 30 centimeters to the right of center. Although atypical of

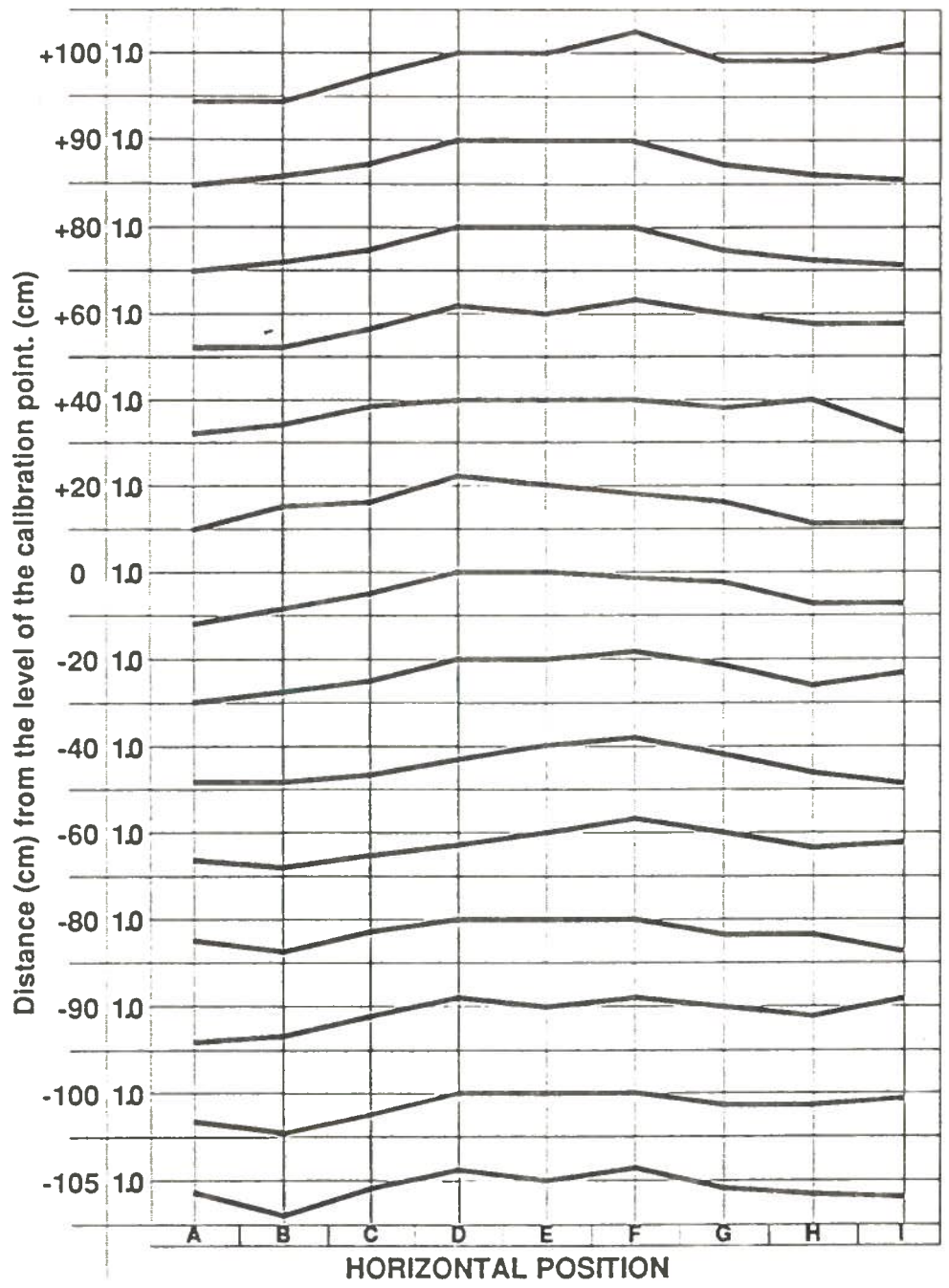

FIGURE 14. Horizontal variation in the treatment plane. Normalizations are made to that value in horizontal position E. The line labeled 1.0 on each row corresponds to the normalized value of 1.00 and the midpoint of a range from 0.90 to 1.10. The lines are to scale for any extensions outside this range.

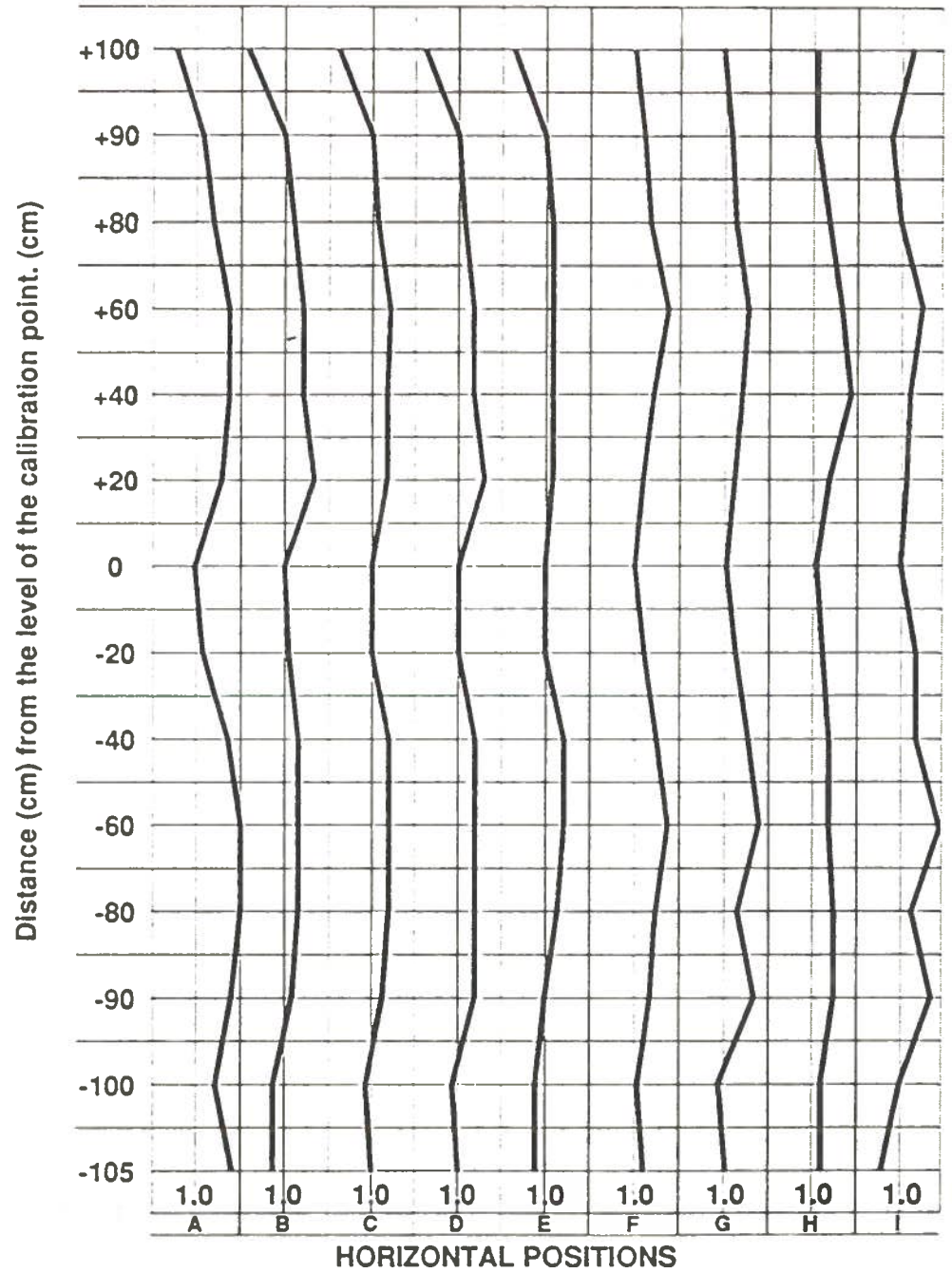

FIGURE 15. Vertical variation in the treatment plane. Normalizations are made to that value at the level of the calibration point. The line labeled 1.0 on each column corresponds to the normalized value of 1.00 and the midpoint of a range from 0.90 to 1.10. The lines are to scale for any extensions outside this range.

the described pattern of central uniformity, Column F of Figure 15, which is 10 centimeters to the right of center, contains the highest average of normalized values for a column or row which is comparable to the study of the Report. It is felt that because the value just mentioned in this study and the AAPM value differ by only 0.4%, that the values on Table 5, Figure 14, and Figure 15 is what is to be expected and should be considered acceptable. When all optical density values of Table 5 are normalized to the calibration point, the smallest and largest of the normalized values are 0.85 and 1.07. The normalized value of the mean optical density obtained from all values in columns B through H is 0.98. The values obtained from the normalization of the mean optical density of each column to the optical density of the calibration point result in values of 0.92, 0.93, 0.96, 1.01, 1.01, 1.02, 0.98, 0.96, and 0.96, respectively, for columns A through I consecutively. Coffey et al. (1982) documents a field uniformity of ±8.9% when using 9 MeV electrons.

C. Beam Characteristics and Output

Beam characteristics were analyzed using the Radiation Associates water phantom and a clear SCRAD polystyrene phantom. The beam was analyzed at 2 meters from the isocenter at the position of the scattering panel and in the treatment plane behind the scatterer. Data for both a horizontal beam and the $+19^0/-19.6^0$ dual angle were collected at the treatment plane while only horizontal beam data were collected at the position of the scattering panel. Figures 16–18 show the ionization versus depth curves. Table 6 summarizes the beam characteristics required for dosimetric calculations. Relative optical densities versus

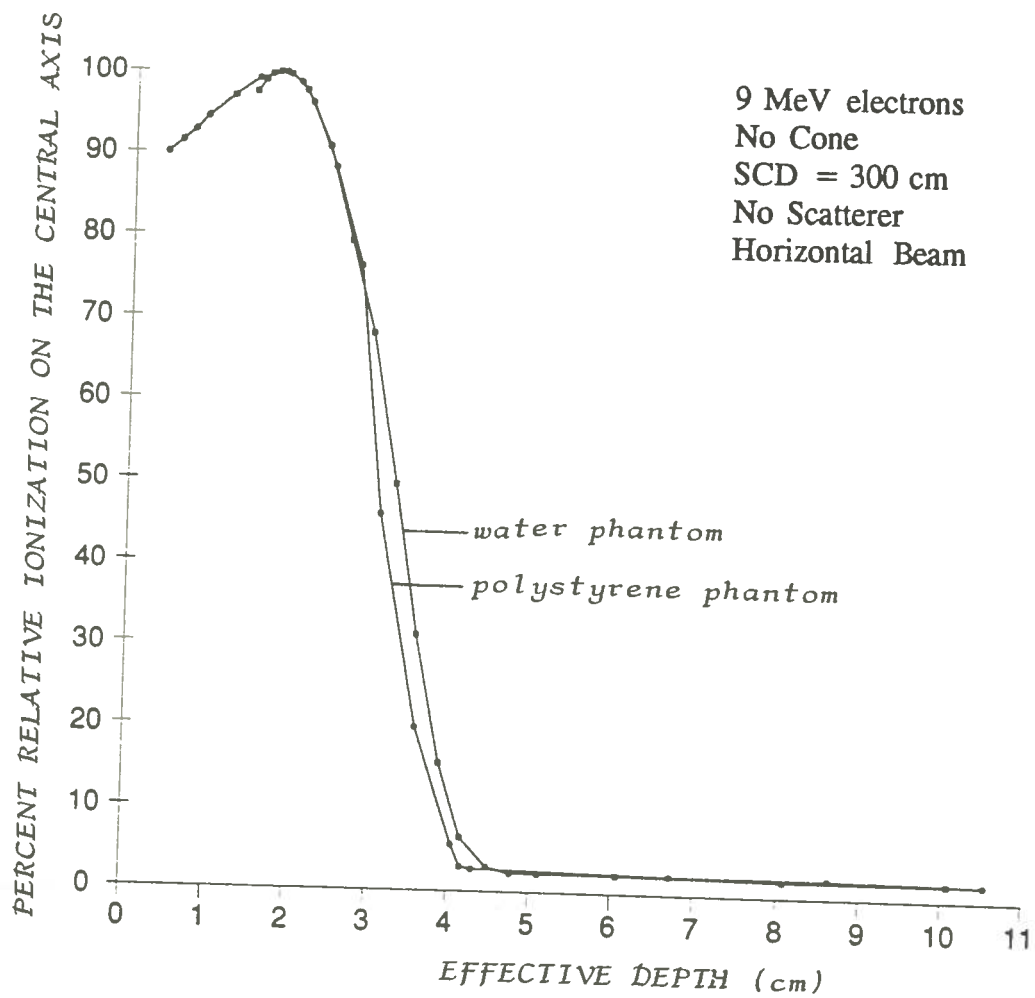

FIGURE 16. Percent relative ionization versus depth curves in water and polystyrene phantoms 200 cm from the isocenter, the location of the scattering panel for a horizontal beam.

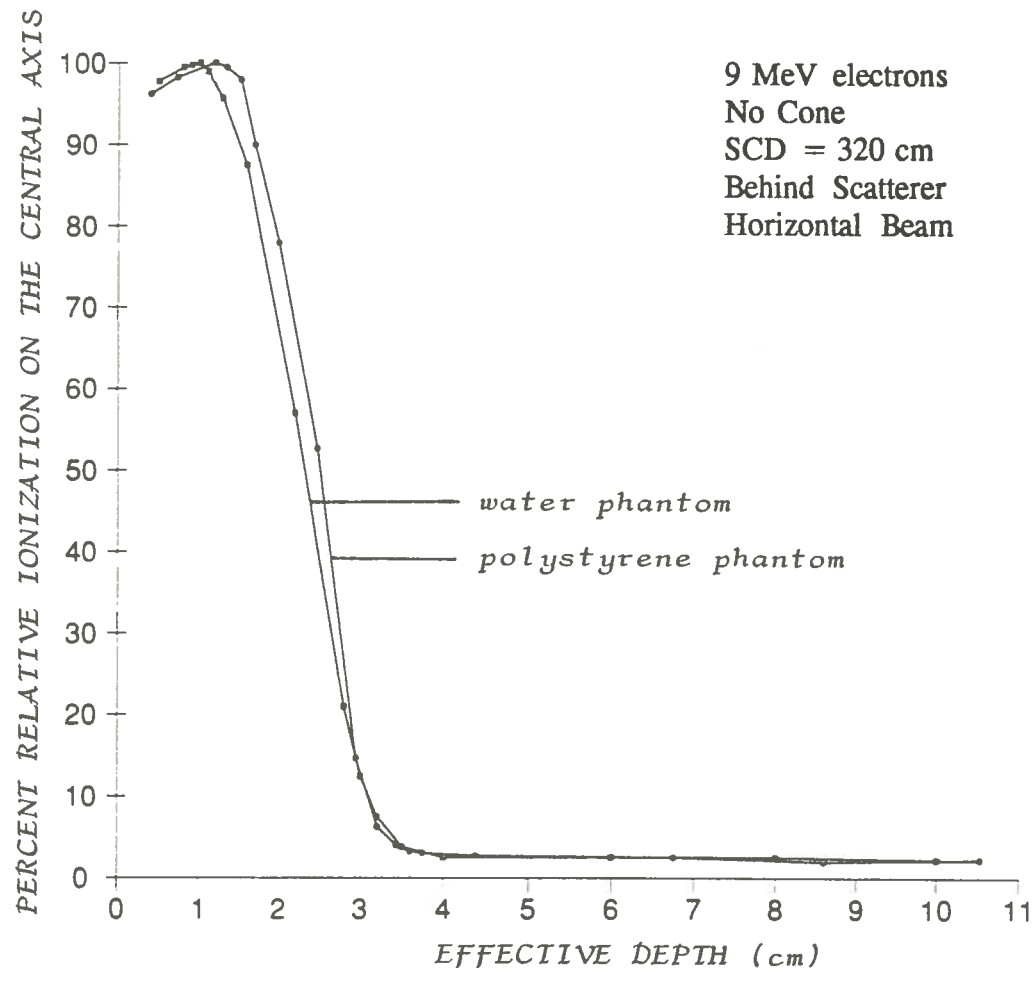

FIGURE 17. Percent relative ionization vs. depth curves in water and polystyrene phantoms behind the scattering panel at the calibration point. The beam is horizontal.

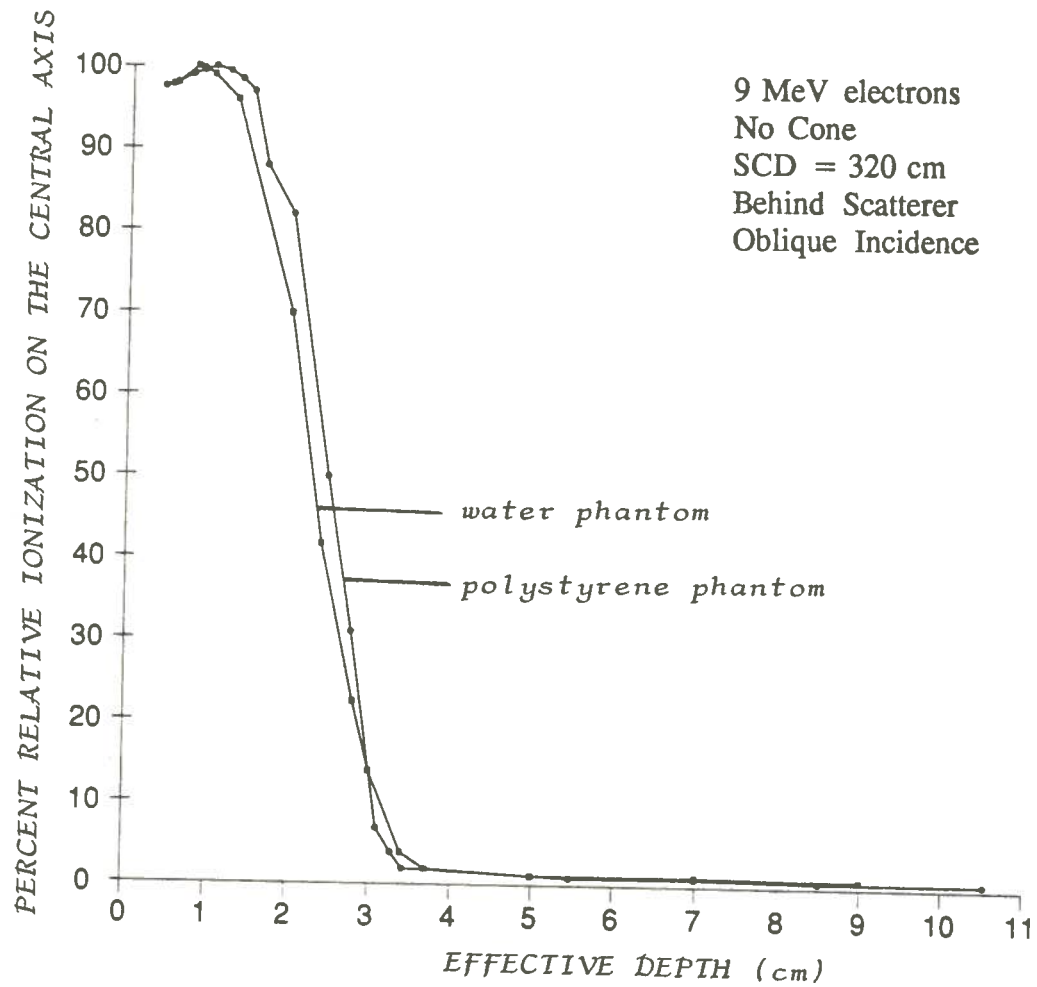

FIGURE 18. Percent relative ionization versus depth curves in water and polystyrene phantoms behind the scattering panel at the calibration point. The dual angle, $+19^0/-19.6^0$, was utilized.

Table 6

9 MeV electron beam characteristics for the geometries investigated.

CONDITIONS	Distance of the Phantom from Source (cm)	Beam Angle	Phantom Material	$\bar{E}_0$ MeV	$\bar{E}_{d_{max}}$ * MeV	d_{max} (cm)	d_{50} (cm)	R_p (cm)	d_{90} (cm)	X-ray Contamination (%)	Output (cGy/MU)
HORIZONTAL BEAM											
No Scatterer	300	270	water	7.7	4.3	1.8	2.6	3.3	4.1	2.0	0.102
(no cone)	300	270	polystyrene	7.0	3.8	1.8	2.6	3.1	3.9	2.6	0.097
HORIZONTAL BEAM											
Behind Scatterer	320	270	water	5.4	3.7	1.0	1.5	2.3	3.1	3.7	0.080
(no cone)	320	270	polystyrene	5.6	3.4	1.2	1.7	2.5	3.1	3.7	0.082
DUAL ANGLE BEAM											
Behind Scatter	320	$+19^0/-19.6^0$	water	5.4	4.1	0.8	1.5	2.3	3.3	2.3	0.037
	320	$+19^0/-19.6^0$	polystyrene	5.6	3.8	1.0	1.7	2.5	3.1	2.3	0.037
	320	$+19^0/-19.6^0$	wax-water and film	5.4	4.8	0.4	0.9	2.4	3.5	--	0.032

* $\bar{E}_{d_{max}}$ refers to the mean electron energy at the depth of maximum dose.

depth were obtained with the use of the wax-water phantom, and the beam characteristics are included in Table 6. Also, the output as determined from the XV2 film (Table 5), was obtained from the optical density on the film strip located at the calibration point on the plywood whereas the other beam characteristics were determined with the use of the wax-water phantom.

Several significant observations can be made from Table 6. Except for the wax-water phantom, all phantoms had a flat surface. Essentially the same results are obtained using either water or polystyrene as phantom materials. Niroomand-Rad et al. (1986) states that the dose distribution is primarily dependent upon the electron energy but is affected by beam angle, size and shape of the phantom and position in the treatment plane. Upon examination of the horizontal beam, $\bar{E}_0$ and $\bar{E}_{d_{max}}$ show decreases of 1.85 MeV and 0.5 MeV, respectively, with the insertion of the scatterer into the beam and an additional 20 cm distance. d_{max} and R_p values show decreases of 0.7 cm and 0.9 cm, respectively. The insertion of the scatterer reduces the output (cGy/MU) by 19%. Angulation of the gantry provides little change in $\bar{E}_0$ and $\bar{E}_{d_{max}}$. The output shows a 54.3% decrease from 0.082 cGy/MU to 0.037 cGy/MU. A 50% reduction in the d_{max} value of 0.8 cm is observed with the use of the wax-water phantom and beam angulation. This reduced value is responsible for the increase in $\bar{E}_{d_{max}}$. The nature of this reduction is explained in the "*Determination of the Depth of Maximum Dose on a Cylindrical Wax-Water Phantom*" section.

Karzmark et al. (1960) reported a pronounced photon contamination which is

centrally located within electron fields. The rationale of gantry angulation when utilizing the dual angle is not only for vertical dose uniformity but also to direct the centrally peaked photon contamination above the head and below the feet (Page et al. 1970). Douglas (1983) states an increase in photon contamination by inserting a polystyrene scatterer into the beam, and White (1983) documented 2.5% less photon contamination by placing the polystyrene scatterer near the phantom surface as compared to its location at the collimator face. Both of these findings are supported by Grollman et al. (1965) and Kumar et al. (1977). This study shows an increase in the photon contamination of 1.4% with the insertion of a 0.6 cm polystyrene scatterer into the horizontal beam at 300 SSD. The photon contamination of 2.3% for a dual field in this study is acceptable. Angulation results in a reduction of the photon contamination by 1.4% below that of the horizontal beam. Coffey et al. (1982) document photon contamination of 2.6% with 9 MeV electrons and a 0.6 cm polystyrene degrader. Bjarngard et al. (1977) reported photon contamination of 2.5% with 7 MeV electrons. Table 8, given in the next section, shows the contribution of each position to the total electron dose of a treatment cycle and proves that the electron dose at any location on the body is delivered by three dual fields. However, the dosage to the same point due to photon contamination is delivered by six fields in this technique. Therefore, the total photon dosage to the skin in a treatment cycle is almost twice the percent photon contamination given for one dual field. The photon contamination given on Table 6 is 2.3% so it follows that the maximum dosage delivered by photons is 4.6%

of the prescribed dose. Holt and Perry (1982) use the same logic in their determination of the bremsstrahlung component received by a patient.

D. Single Dual Field Fractional Contribution

A cylindrical nalgene water tank having a 30.5 cm diameter was supported by a plastic turntable mounted on a plastic cart and positioned so that half of the height of the tank was at the calibration point 20 cm behind the scattering panel and then filled with water. Three experiments were conducted to determine individual dual field contribution. Measurements were taken at the six dose maxima locations as explained in the ***Materials and Methods*** section. The fraction contribution was then calculated. This value is the reciprocal of the value of "B" in the AAPM Report #23 (1988) which is explained as a modifying factor accounting for field overlap. The reciprocals of the "B" values given as a typical range are 0.323 to 0.400. Table 7 shows the XV2 film derived values of this study to fall near the middle of this range. The TLD derived value of 0.3163 is 2.2% below the lowest value of the typical range. Similarly, Vonderheid and Micaily (1987) apply the symbol "F" recognizing the necessity of accounting for the overlap of fields when calculating average skin dose. Niroomand–Rad et al. (1986) express a similar value, the "summed dose factor" which relates the maximum dose required by a cylindrical phantom at the calibration point from a horizontal beam to the dose received from a six-field method which utilizes beam angulation. It was found that increasing the phantom size decreases the summed dose factor. It follows that the fractional contribution value of this study should behave in the reverse manner of decreased

TABLE 7

Results of investigations to determine the fractional contribution of one dual field. Film readings are optical densities. TLD readings are in cGy (960 MU/dual field). Film vs. TLD.

(Trial 1: 200 MU/dual field*; Trial 2: 300 MU/dual field)

Method	Total Contribution of Six Dual Fields						Results from One Dual Field	Fractional Contribution	Output from One Dual Field (cGy/MU)
	POSITION								
	1	2	3	4	5	6			
XV2 Film									
Trial 1	0.62	0.62	0.61	0.60	0.61	0.61	0.215	0.3515	0.0322
Trial 2	0.90	0.88	0.85	0.92	0.83	0.87	0.32	0.3657	0.0327
TLD-100 Flat Packs	100	96	97	96	99	100	31	0.3163	0.0323
					AVERAGES			0.3445	0.0324

*MU/dual field refers to the total number of monitor units (MU) used for both fields in which one field is angled above the horizontal and the other is angled below the horizontal.

fractional contribution accompanying decreased phantom radii because decreased phantom radii means greater beam obliquity. The calculations of output from one dual field and fractional contribution from the data show the values to be in agreement. The determination of fractional contribution with the use of the ionization chamber is not recommended by the AAPM Report #23 (1988).

1) Determination with XV2 Films

Four film strips were wrapped around the outside of a water-filled nalgene tank at the level of the calibration point as shown in Figure 5, and exposed to the six dual field $+19^0/-19.6^0$ technique using 200 MU/dual field and 300 MU/dual field for trial 1 and trial 2, respectively (Table 7). The values of output from one dual field which were calculated from XV2 film data, given in Table 7, show a 1.6% difference between the two trials. The results from ionization chamber data, shown on Table 8, have a 2% difference between the two trials. The data indicate that output measurements are reproducible within 2% using film and an ionization chamber. However, there is a difference of 5.8% between the film and the chamber.

2) Determination with TLD

The calculation of output on Table 7 and Table 8 from TLD data results in a 2.2% difference between their values. When comparing values from TLD data with that from XV2 film and ionization chamber, the values have percentage differences of 1.6% and 7.8%, respectively, indicating a better agreement between TLD and film than between either of these and the

TABLE 8

Results showing the contribution of dosage to the phantoms at each position in the cycle. Ionization chamber (PTW N233641 #693) data are electrometer readings. TLD data are doses in cGray (980 MU/d.f.). TLD vs. Ionization Chamber.

(Trial 1: 800 MU/d.f.;** Trial 2: 1200 MU/d.f.)

Method	Contribution of One Dual Field to Each Position						Total Dose from One Cycle (cGy)	Dose, One Dual Field at Position 1 (cGy)	Output from One Dual Field (cGy/MU)
	POSITION								
	1	2	3	4	5	6			
Ionization Chamber									
Trial 1	0.330	0.146	0.002	0.002	0.002	0.122	50.0	27.3	0.0341
Trial 2	0.494	0.306	0.009	0.007	0.009	0.342	98.6	41.7	0.0348
TLD	31	31	1.1	0.5	1.3	32	99.0	31.0	0.0316
F.D.*	31.3%	31.3%	1.1%	0.5%	1.3%	32.3%			

*F.D. = fractional dose at different positions (TLD).

**MU/d.f. refers to the total number of monitor units (MU) used for both fields in which one field is angled above the horizontal and the other is angled below the horizontal.

ms at each position in the
e electrometer readings.
ization Chamber.
U/d.f.)

ose, One ual Field Position 1 (cGy)	Output from One Dual Field (cGy/MU)

3
7 0.0341
0.0348

0.0316

d is angled above the

chamber. Table 7 shows that the average dose received at the surface is 2% below the expected dose of 100 cGy.

E. Dose Fraction With Position

A fractional contribution was obtained for each position (see Table 8). The scheme of TLD placement is given in Figure 11. Table 8 shows that TLD and ionization chamber data do not agree on the dose received by each position. However, it does indicate that the entire dose is delivered in the three positions which are toward the beam and each of these positions contributes about one-third of the total dose. As shown on Table 7, rotation of the phantom results in a uniform dose in all positions because each position becomes exposed to the same beam incidence and amount of radiation over the course of the treatment cycle. Trial 2 on Table 7 indicates that we can have an 11% variation between positions even with the good geometry of the tank. We should expect larger variations with a patient because of body surface irregularities. The effective depth of 0.8 cm was found not to be the depth of maximum dose for the wax-water phantom using this technique. The lower ion chamber values for positions #3 through #5, compared to the TLD values, can be explained by the obliquity of the phantom which makes chamber measurements more unreliable.

F. Determination of the Depth of Maximum Dose on a Cylindrical Wax-Water Phantom

A six dual field series of exposures was made using 300 MU/dual field rotating the phantom in the 60-degree increments between each dual field. A relative

optical density versus depth curve was generated from the measured optical density values (Figures 19 and 20). Optical densities observed around the periphery of the film yield a series of 6 optical density maxima and minima which alternate with a 60-degree periodicity corresponding to the 60-degree increments of phantom rotation (Figure 21). The dose minima are offset 30 degrees from the dose maxima as expected. Figure 20 shows the typical curves for a dose maximum (60^0) and a dose minimum (270^0). The greatest depth containing a uniform, maximum optical density was 6-mm. A greater frequency of uniform maximum optical densities were displayed at depths of 3-mm and 4-mm. For this experiment, the investigator feels that the most likely error in the determination of d_{max} would result in a value that is too shallow. Protrusion of a film edge beyond the phantom can more easily be observed than film edge concavities beneath the surface of the phantom. It is concluded that the value of d_{max} to be at least 4-mm and may extend to 6-mm. Because it is difficult to cut film into a perfect circle, a reasonable error in depth may be as much as 2-mm in this experiment. This range of d_{max} values should not be expected to agree with the d_{max} of Figure 18. The geometry of Figure 18 concerns a flat surface where as the wax-water phantom possesses a concave surface with respect to the beam. A superficial shift in the d_{max} was displayed as expected. Table 6 contains beam characteristics for the wax-water phantom derived from Figure 20 and serve only to corroborate chamber derived values. The exception is the d_{max} value. There is agreement between the values for $\bar{E}_0$, $\bar{E}_{d_{max}}$, d_{50}, R_p, and output. An estimate of the photon contamination, not included on Table 6, is made

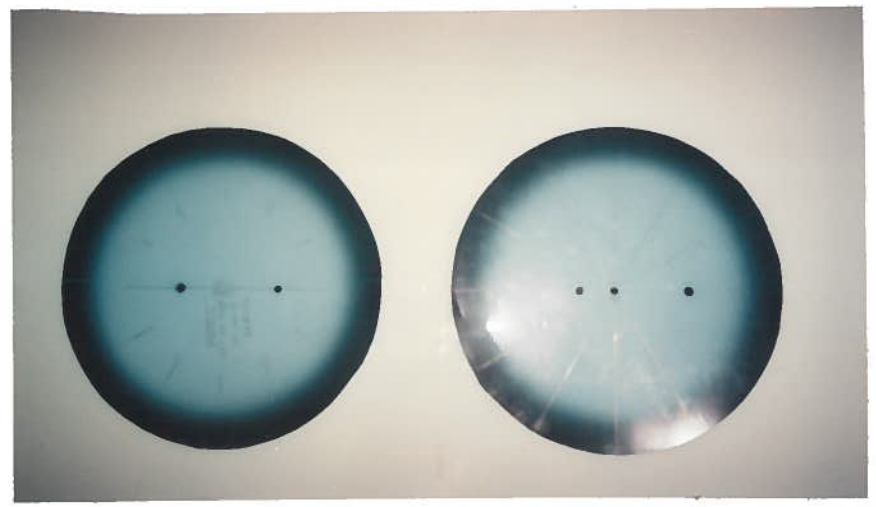

FIGURE 19. Photograph displaying the depth of exposure to XV2 film placed in the wax-water phantom. Both films are 30.5 cm in diameter. The relative optical density versus depth is plotted on Figure 20. The films shown above result from two identical experiments.

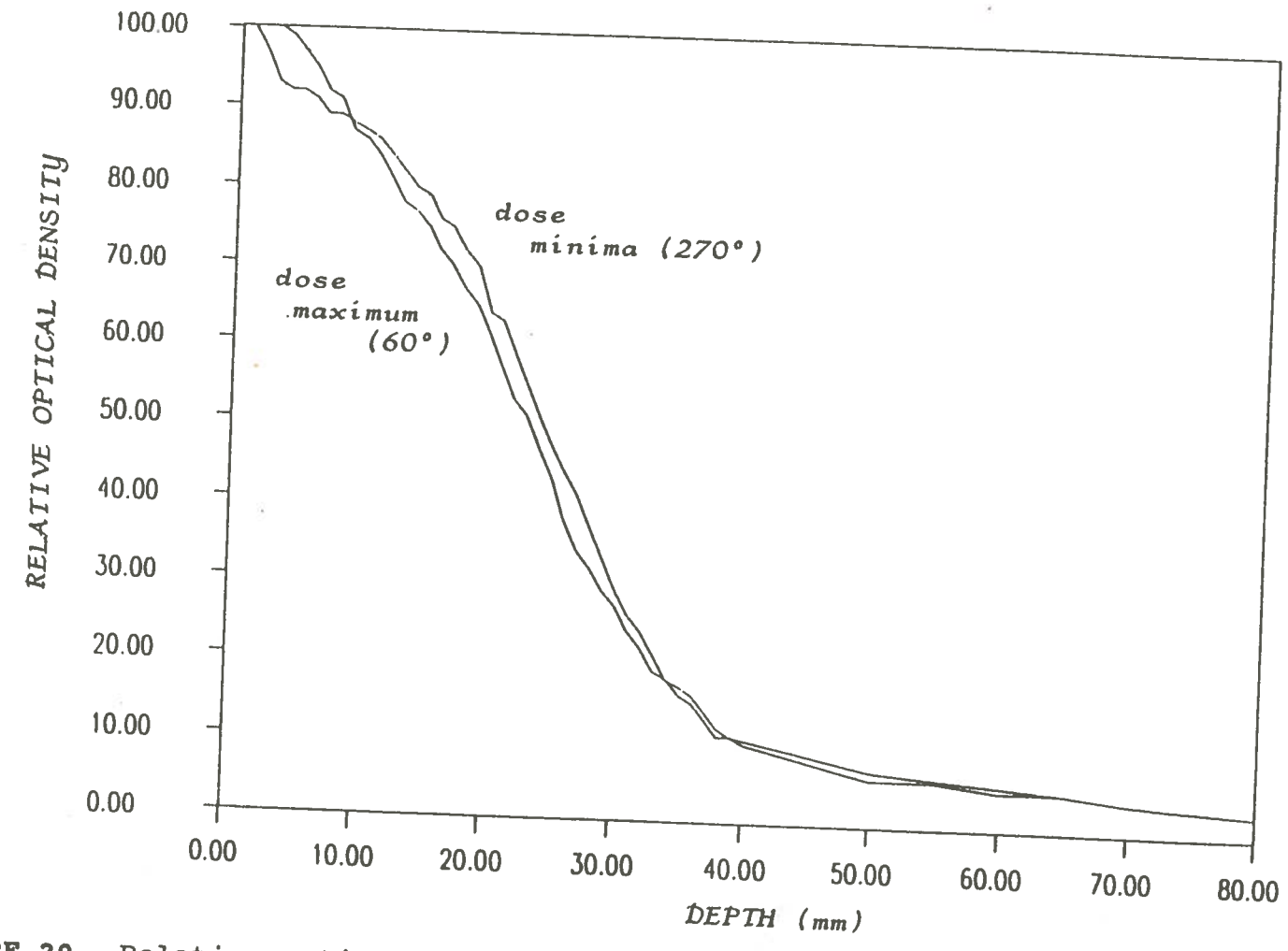

FIGURE 20. Relative optical density versus depth curves from XV2 film in the wax-water phantom. Typical dose maximum and minimum positions encountered following the circumference of the film. Estimation of some beam characteristics were obtained.

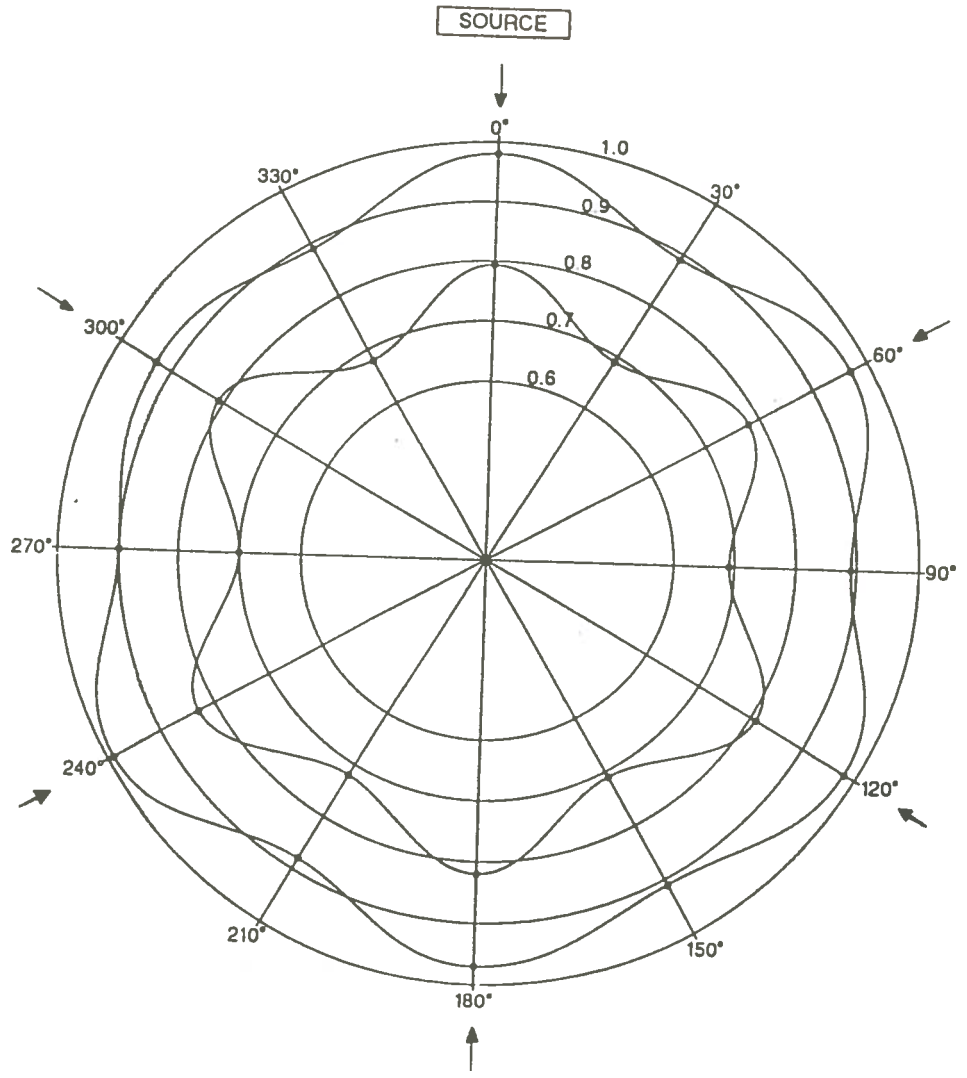

FIGURE 21. Analysis of the optical densities around the periphery of the film at 4 mm from the edge yield a series of 6 optical density maxima and minima which alternate with a 60 degree periodicity. The two trials performed display similar patterns. The arrows identify the locations on the phantom and are placed at the calibration point throughout the cycle of treatment.

from the lowest point on Figure 20 and is 2.6%. Values obtained from a calibrated ionization chamber should be used for all beam characteristics except for the d_{max} value which, in this case, is more accurately evaluated from film in a more geometrically realistic dosimetry phantom. Niroomand–Rad et al. (1986) state that dose distributions depend on electron energy and are significantly affected by beam angle, size and shape of the phantom and its position in the treatment plane. Also stated was that one beam angle is appropriate for all phantom sizes. Bjarngard, et al. (1977) agree by citing no significant difference in depth dose between different phantom radii.

G. Confirmation of a Prescribed Dose

The formula adopted for the calculation of monitor units from a prescribed dose was given in the ***Materials and Methods*** section. TLD-100 envelopes were used in confirming the fractional field contribution obtained with film. The monitor units per dual field required to deliver 100 cGy were calculated to be 960 MU/d.f. and the dosage was confirmed. See Table 7.

A mannequin obtained for the purpose of simulating a patient undergoing this technique was irradiated with both 6 and 9 MeV electrons and having the goal of delivering 200 cGy. A list of the locations of TLD placement and the doses received are given on Table 9. There is a large discrepancy between the goal of 200 cGy and the doses obtained with TLD. In a later experiment, two XV2 film strips were taped onto the mannequin (one on the anterior and one on the posterior) and irradiated with one dual field. The optical densities measured on the posterior or

TABLE 9

Dose in cGy received by TLD-100 flat packs using 6 MeV electrons and by TLD-100 chips using 9 MeV electrons utilizing the six dual field technique. The intentional dose of 200 cGy was not received because the construction of the mannequin did not allow its use as a patient substitute.

LOCATION WAIST LEVEL	6 MEV	9 MEV
a. AP	116	164
b. RAO	122	154
c. Rt	133	151
d. RPO	128	154
e. PA	130	172
f. LPO	140	167
g. Lt	120	151
h. LAO	127	164
Rt femur, midshaft	--	162
Body of sternum	161	179
T-4	164	181
Rt patella	153	169
Rt lower leg, midshaft	134	169
Rt foot, proximal	149	151
C-6	--	181

exiting surface of the mannequin averaged 80% of those measured on the anterior or incident surface. This excludes the use of the mannequin as a patient substitute without further modification to the mannequin. These values may reflect modified in-air doses.

TLD-100 chips were placed on the plywood panel at 30 locations that reflect the area in the treatment plane that would most likely be occupied by a patient (Figure 22 and Table 10). The relative doses to the TLD chips range from 94 cGy to 107 cGy in the area illustrated as the torso of the body. Also, 91 cGy and 98 cGy are displayed at possible locations for a hand. The doses displayed across the torso of the body are within ±7% of the prescribed dose of 100 cGy and within ±9% whenever the hands are considered. Higher doses are seen near the +60 cm and −60 cm positions which reflects the pattern of the unequal dual angle on Figure 13. There is a standard deviation of 3.65% of the mean dose value in that area most likely occupied by a patient. These results fall within the variation given by the AAPM Report #23 of 20%. The output used in calculating the required monitor units to deliver 100 cGy to the surface of the plywood (0.0366 cGy/MU) was that output obtained with the parallel plate chamber at the depth of maximum dose. The doses obtained from the TLD chips averaged 10.6% lower than the expected dose of 100 cGy. The main reason for this deficiency lies in the selection of calibration output used to calculate the number of monitor units to be used. The output of 0.0366 cGy/MU is the output at depth of maximum dose whereas the dose

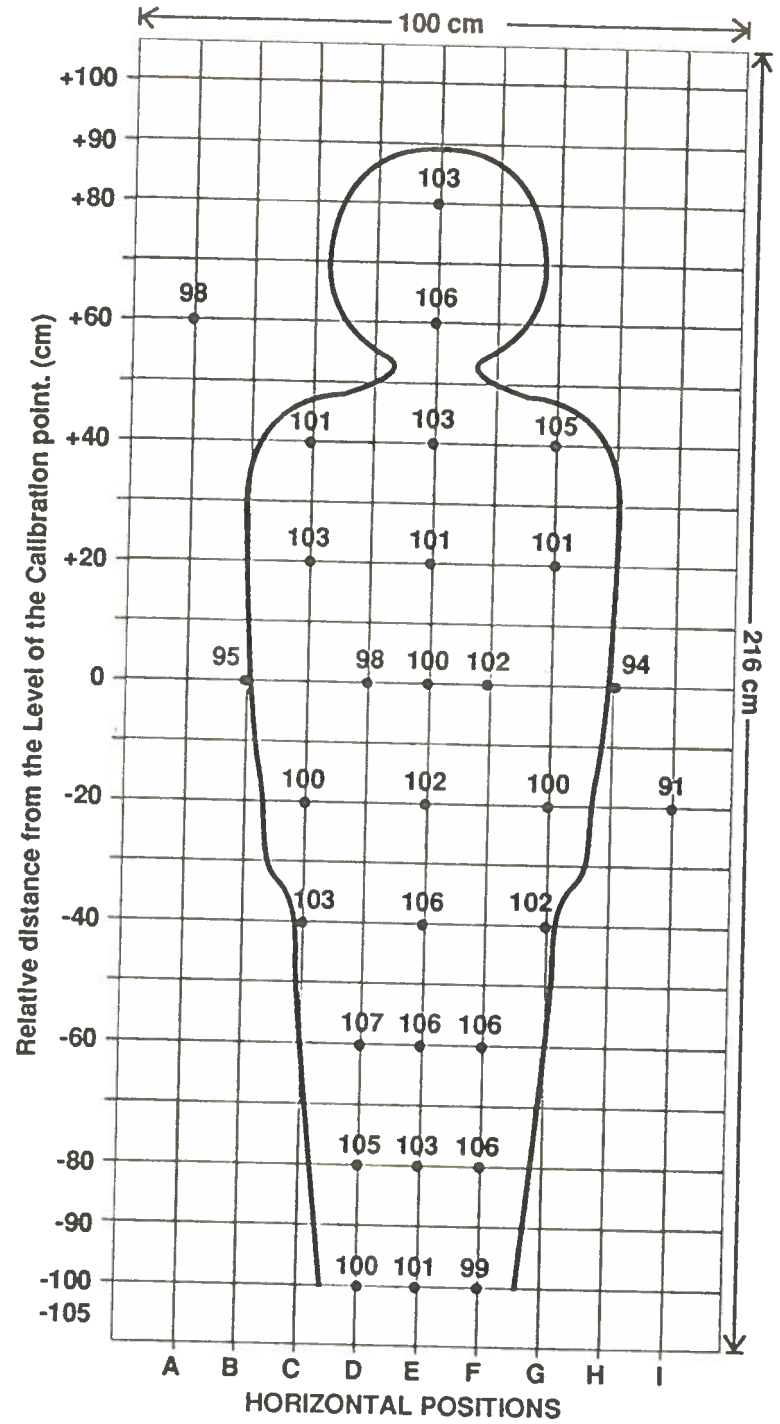

FIGURE 22. Diagram showing relative dose values to TLD chips at locations in the treatment plane most likely occupied by a patient.

is being detected at the surface. Output in the range of those listed in Table 7 for a single dual field would provide 100 cGy, the dose expected.

H. Data for Attenuated Electrons

Relative ionization versus depth curves were generated for the attenuated 9 MeV electrons at 100 cm SSD using 6 x 6 cm^2, 10 x 10 cm^2, 15 x 15 cm^2, 20 x 20 cm^2, and 25 x 25 cm^2 electron cones with square white high impact polystyrene scattering panels taped to the distal apertures of the electron cones. The scattering panel-to-surface distance was 34.9 cm. The output (cGy/MU) which was obtained with and without the scatterer in place along with the other beam characteristics are tabulated in Table 11. The relative ionization curves for each cone are given in Figures 23 through 29. (To avoid confusion of data, it was decided that each cone should have its own graph.) Table 11 shows a generally insignificant change in the values of d_{max}, d_{50}, R_p, $\bar{E}_0$, and $\bar{E}_{d_{max}}$ among the different electrons cones utilizing the 6.4-mm high impact polystyrene scatterer. Values obtained for the 25 x 25 cm^2 cone with the 5-mm acrylic scattering panel attached to the cone are only slightly lower than the comparable values obtained with the high impact polystyrene scatterer. Results of the 25 x 25 cm^2 cone without a scatterer attached show that with the addition of the scatterer there are decreases in the d_{max}, d_{50} and R_p values by about the same amount as the thickness of the scattering panel. The high impact polystyrene and acrylic panels decreased the $\bar{E}_0$ value by 1.0 MeV and 1.5 MeV, respectively. A comparison of the water phantom data for the 25 x 25 cm^2 electron cone with no scatterer at 100 cm SSD versus the data obtained with no cone and

TABLE 11

Tabulations of dosimetric parameters used for the electron cones available with the Clinac 18. The gantry was placed in the beam-down position over the Med-tech water phantom. 100 SSD, 9 MeV electrons.

Electron Cone (cm^2)	Beam Descriptors with 6.4 mm White High Impact Polystyrene Scatterer in Place							WITHOUT Scatterer Output (cGy/MU)
	d_{max} (cm)	d_{90} (cm)	d_{50} (cm)	R_P (cm)	$\bar{E}_0$ (MeV)	$\bar{E}_{d_{max}}$* (MeV)	Output (cGy/MU)	
6	1.2	2.0	2.8	3.7	6.5	4.4	0.887	0.907
10	1.2	2.0	2.8	3.5	6.4	4.2	1.016	1.008
15	1.2	2.0	2.7	3.6	6.2	4.2	1.082	1.078
20	1.1	2.0	2.7	3.6	6.3	4.3	1.182	1.160
25	1.0	2.2	2.7	3.7	6.3	4.6	1.159	1.150
Without scattering panel:								
25	1.5	1.8	3.2	4.1	7.3	4.7		1.150
With 0.5 cm acrylic scattering panel:								
25	0.9	1.6	2.5	3.4	5.8	4.3	1.148	

*$\bar{E}_{d_{max}}$ is the mean electron energy at the depth of maximum dose.

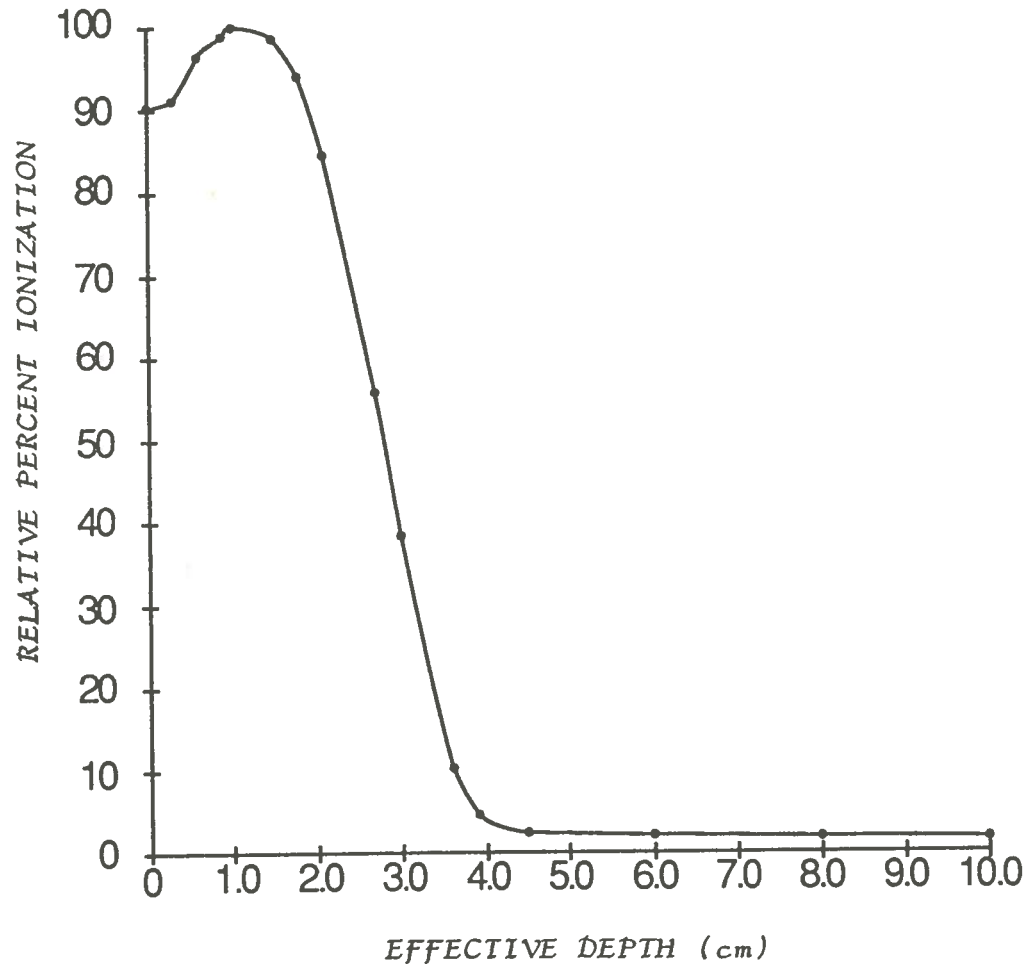

FIGURE 23. Relative percent ionization versus depth (cm) in water for the 6 x 6 cm electron cone. Nine (9) MeV electrons. X-ray contamination, 3.48%. White high impact polystyrene scattering panel is 12.3 cm x 12.3 cm x 0.635 cm. 100 cm SSD.

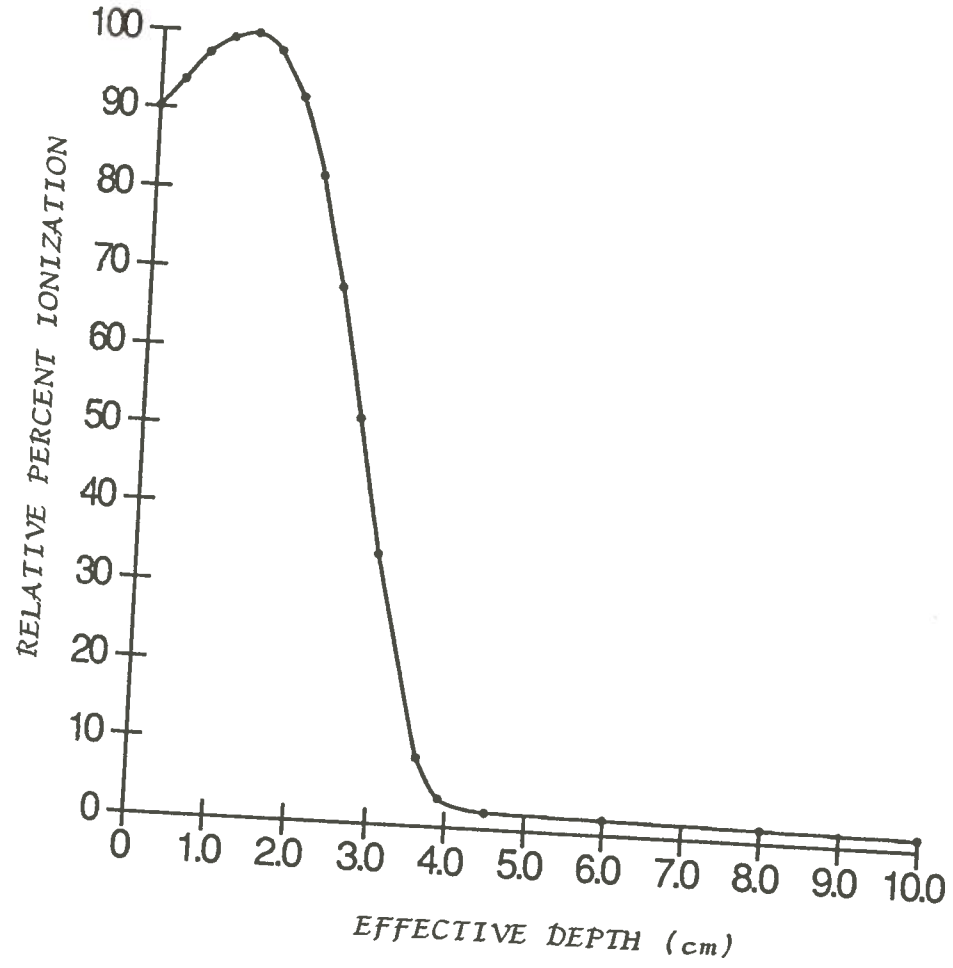

FIGURE 24. Relative percent ionization versus depth (cm) in water for the 10 x 10 cm^2 electron cone. Nine (9) MeV electrons. X-ray contamination, 3.48%. White high impact polystyrene scattering panel is 16 cm x 16 cm x 0.635 cm. 100 cm SSD.

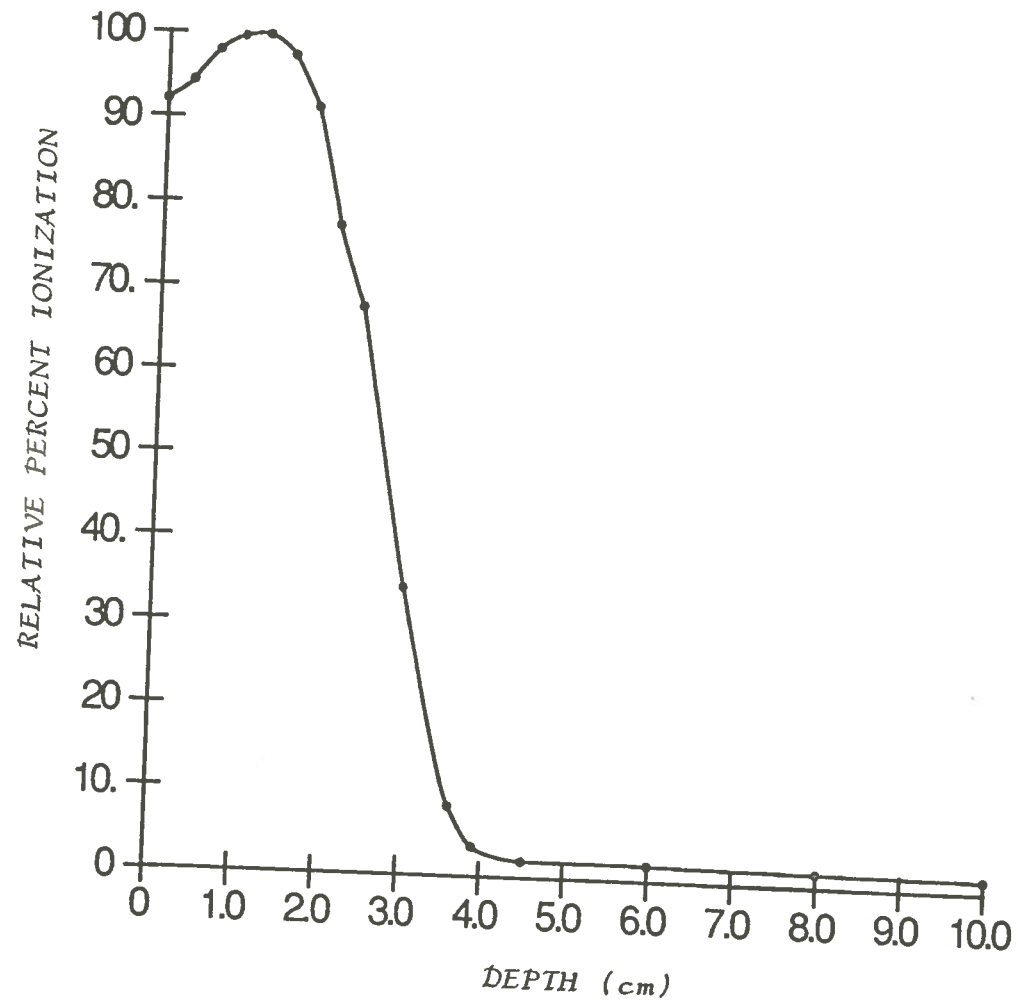

FIGURE 25. Relative percent ionization versus depth (cm) in water for the 15 x 15 cm^2 electron cone. Nine (9) MeV electrons. X-ray contamination, 2.9%. White high impact polystyrene scattering panel is 21.3 cm x 21.3 cm x 0.635 cm. 100 cm SSD.

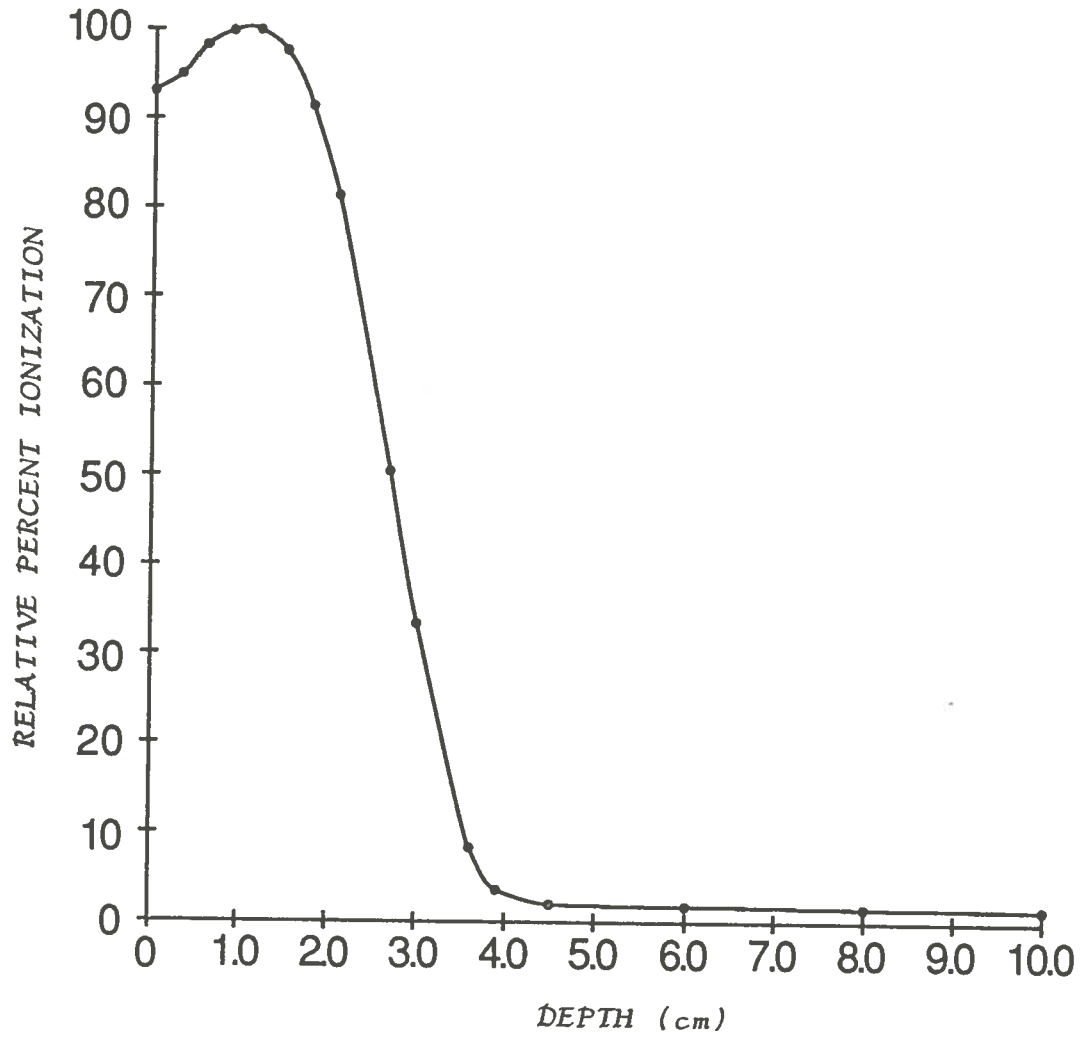

FIGURE 26. Relative percent ionization versus depth (cm) in water for the 20 x 20 cm^2 electron cone. Nine (9) MeV electrons. X-ray contamination, 3.0%. White high impact polystyrene scattering panel is 25.5 cm x 25.5 cm x 0.635 cm. 100 cm SSD.

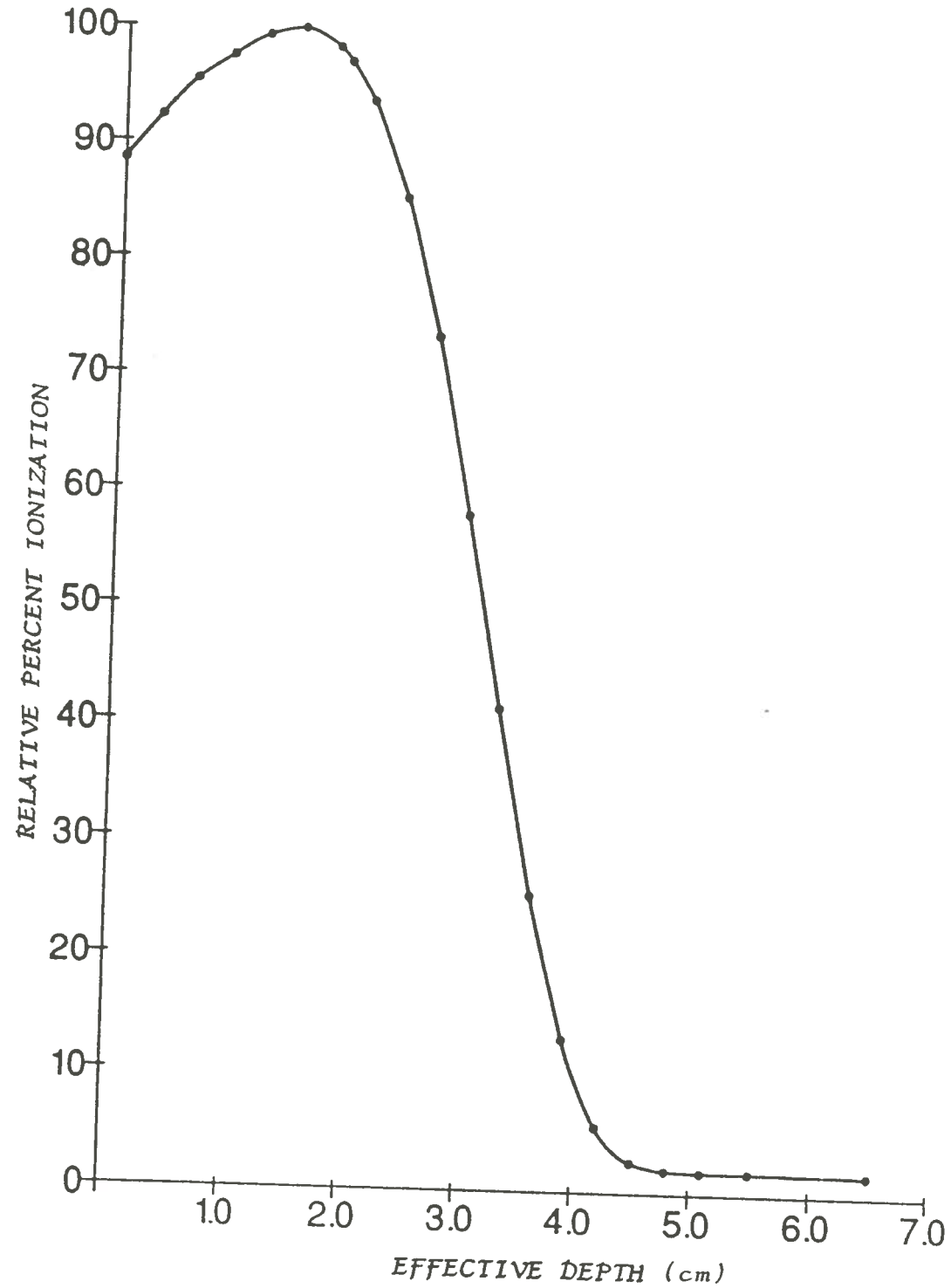

FIGURE 27. Relative percent ionization versus depth (cm) in water for the 25 x 25 cm^2 electron cone. Nine (9) MeV electrons. No scattering panel. X-ray contamination is 2.6%. 100 cm SSD.

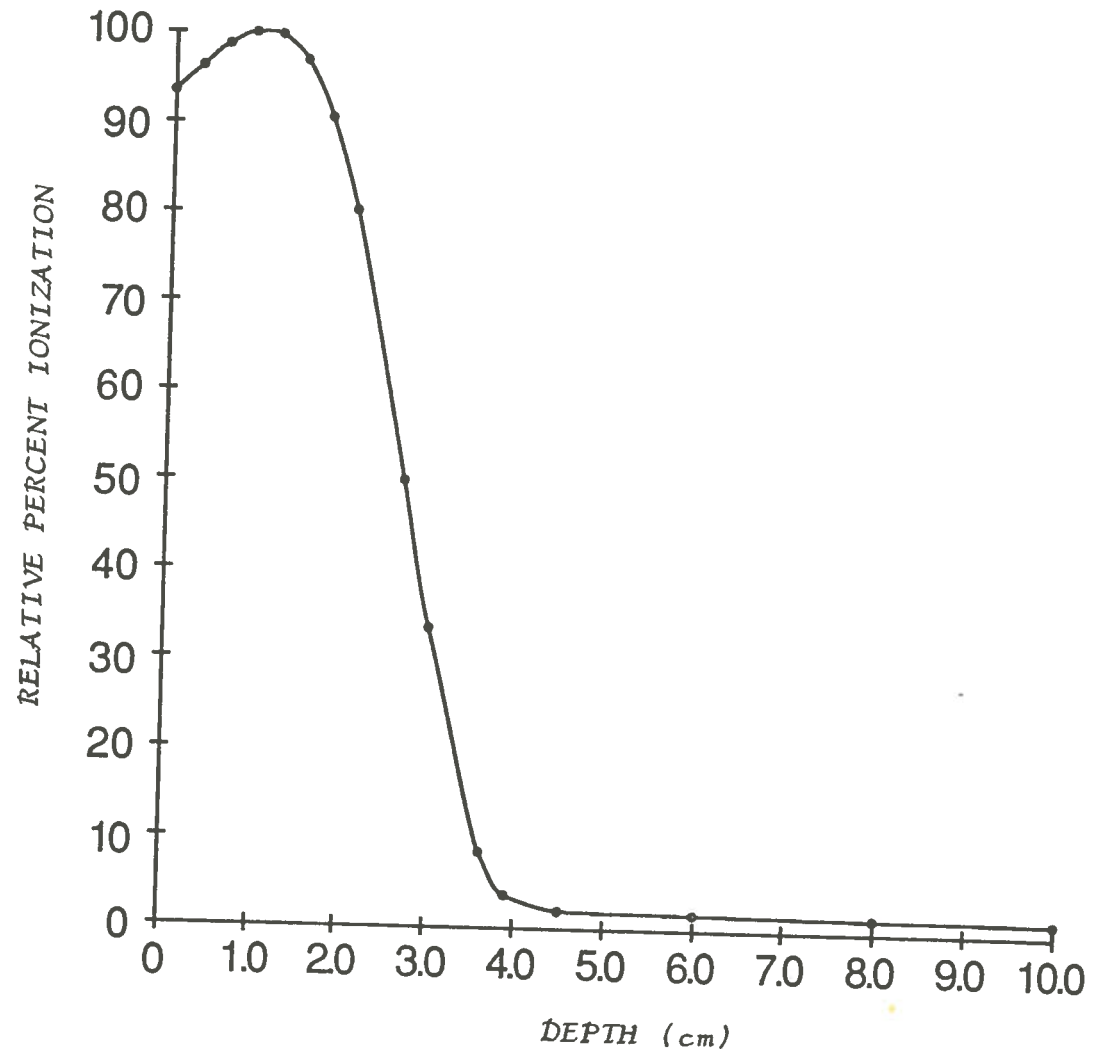

FIGURE 28. Relative percent ionization versus depth (cm) in water for the 25 x 25 cm^2 electron cone. Nine (9) MeV electrons. X-ray contamination, 2.7%. White high impact polystyrene scattering panel is 30 cm x 30 cm x 0.635 cm. 100 cm SSD.

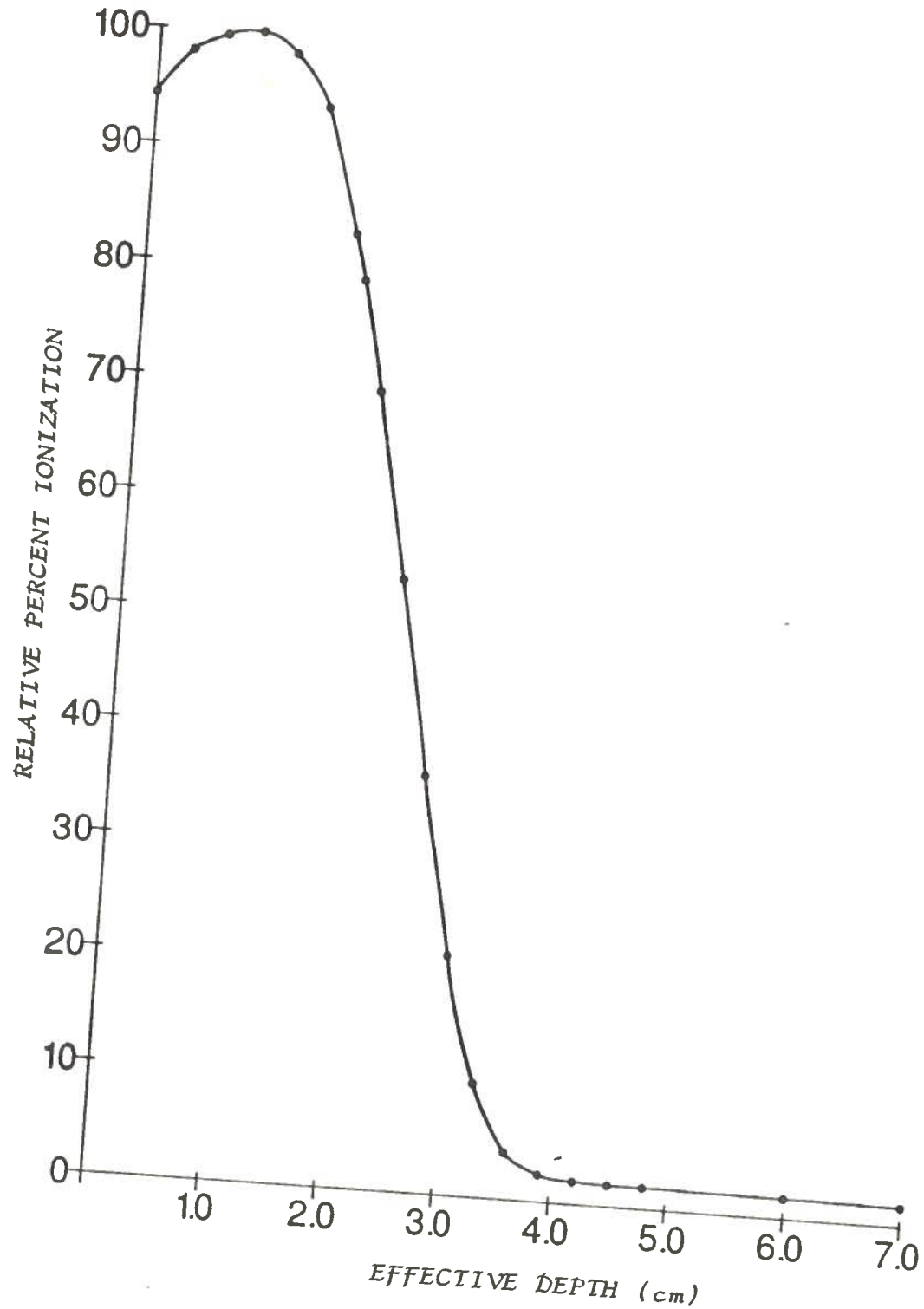

FIGURE 29. Relative percent ionization versus depth (cm) in water for the 25 x 25 cm^2 electron cone. Nine (9) MeV electrons. Electron cone with 0.5 cm acrylic scattering panel attached. X-ray contamination is 2.8%. 100 cm SSD.

no scattering panel at 300 cm SSD from Table 6 shows no significant change in $\bar{E}_0$, $\bar{E}_{d_{max}}$, d_{50}, and R_p. The output decreases by a factor of eleven under these conditions. With the above comparison remaining the same except for the insertion of the scattering panel into the beam at 300 SSD, there is a resulting decrease in both $\bar{E}_{d_{max}}$ and $\bar{E}_0$ values of 0.9 MeV from 4.6 MeV and 6.3 MeV to 3.7 MeV and 5.4 MeV, respectively. The value of d_{max} decreases by 0.5 cm and both d_{50} and R_p decrease about 1.0 cm. Table 11 shows the output values obtained without the scatterer attached to the cone to be similar to those obtained with the scatter.

I. Error Analysis

Errors associated with this 9 MeV electron total skin technique are classified as determinate or indeterminate errors. Determinate errors are regarded as constant or systematic errors which may be reduced with vigilant experimental design and trial runs whereas indeterminate errors are random and observational in nature (Chase and Rabinowitz, 1967).

1) Determinate Errors

Determinate errors outlined here pertain to errors in experimental setup, equipment variability and temperature changes. One initial task of the setup was the suspension of a plumb bob from the isocenter to the floor before fixing the position of the scattering panel 200 cm away. Because the plumb bob was hand held, 3 mm (3mm/3000 mm) is allowed resulting in a 0.10% error. After the placement of the scattering panel this location was marked by a line drawn on a piece of masking tape which was stuck to the carpet. Some slight

movement of the tape due to daily wear and tear was observed over the course of this study. Careful attention was paid to these marks when positioning the platform and a 5 mm variability may have resulted in a 0.25% (5/2000) error. The placement of both the water and plastic phantoms were set at specific distances behind the scattering panel and secured with strong tape. Polystyrene sections were withdrawn from the phantom and inserted when changing the depth of measurement possibly changing the position of the phantom. Although the position was checked regularly and particularly when movement was thought to occur, a 3 mm (3 mm/200 mm or 1.5%) error may have occurred. The author feels that distance errors behind the scattering panel are important to consider. The measuring tape used for determining the location of the platform was compared to a centimeter ruler, Model 722, obtained from Radiation Products Design (Buffalo, MN) and was found to vary 0.25 mm in 45 cm. The greatest variation found with the rulers used to measure distances behind the scattering panel was 1 mm in 30 cm.

Adjusting the gantry to the horizontal was done using a level but after the horizontal was marked onto the scattering panel, there was slight variability in consistently setting the gantry to this point using the level. The greatest variation experienced was 0.5 cm from the mark. Little shifting of the panel inside the frame of the platform was observed but a 0.25 cm shift in the vertical direction may have been observed when setting up the panel after

marking distances on it. The total angle variation corresponds to a 1.09% (.75/68.9) error.

Errors in the linear accelerator output were monitored by performing output constancy checks before all experiments. The criterion used for constancy checks is 2%. Temperature and pressure corrections were applied to dose calculations and accounted for in the constancy checks.

The developer temperature in the X-OMAT automatic processor was maintained at 35^0C degrees for all films processed. No variation was observed in this temperature. No quality assurance tests are maintained on this processor but the mechanisms are kept clean and no change in the background density was observed before developing the films of each experiment.

The TLD readers used in this study are operated independently by different private concerns. Our provider states that when using a series of TLD-100 powder envelopes with three controls which are irradiated at the suspected doses, error is as low as 4% with his system (Cundiff 1989). Susan Smith (1989) states a 5% error in doses to the TLD chips.

2) Indeterminate Errors and Calibrations of XV2 Film and TLD-100 Chips

SAS/STAT (1985) programs were utilized in evaluating XV2 film and TLD-100 calibration data. The data was analyzed using a least squares linear regression model with the variables arranged in the slope-intercept form for the equation of a line, $y = mx + b$, where m is the slope and b is the y-intercept. When performing the experiments, exposures were made so that

optical densities obtained were within the linear portion of a nontransformed film response. The percentage change in the slope (m) values reflects random changes in the film or TLD responses whereas the y-intercepts (b) reflect systematic conditions such as developing temperature. The SAS/STAT program provides data evaluations in regard to how well the regression equation fits the observed data (r^2 values) and to the probability of the mathematical relationship being a random one (Pr value).

[a] Kodak XV2 Film Calibration

Calibrations of both 6 and 9 MeV electrons were performed twice and evaluated. ICRU 35 (1984) states that film response over a range of electron energies can be expected to have little variation and the calibrations made in this study confirm this with this batch of film. Insignificant differences were shown between the two calibration curves generated using the 6 and 9 MeV electron energies. The pattern of the residual values versus dose suggested nonlinear relationships for both electron energies. Reciprocal transformations were made to make essentially linear models linear. These results are presented in Table 12. The extremely low Pr values reflect a highly significant regression. The r^2 values show how the regression fits the observed data. The values of r^2 may range from zero to 1.000 with 1.000 corresponding to a straight line. The equations produced by the SAS/STAT program relating optical density to dose having the greater r^2 values are given as follows:

TABLE 12

Statistical parameters determined by the S.A.S./S.T.A.T. program for least squares curve fitting of optical densities onto dose in the calibration of XV2 film.

9 MeV	Experiment 1	Experiment 2	% Change
b	0.21240211	0.19240589	9.41
m	28.46179578	28.46179578	0.28
r^2	0.9998796	0.999877	0.01
Pr	0.0001	0.0001	0

6 MeV	Experiment 1	Experiment 2	% Change
b	0.21208908	0.21503953	1.39
m	28.2942727	28.54083408	1.03
r^2	0.999272	0.999579	0.03
Pr	0.0001	0.0001	0

$$6\ MeV: \quad \frac{1}{Optical\ Density} = 0.21 + 28.54\ \frac{1}{dose}$$

$$9\ MeV: \quad \frac{1}{Optical\ Density} = 0.19 + 28.46\ \frac{1}{dose}$$

Mota, et al. (1990) underscores the importance of curve fitting in the calibration of film. The calibration curves are given in Figures 30 and 31.

[b] TLD-100 (LiF) Chip Calibration

Two calibrations using 6 MeV electrons were performed with linear regressions of the TLD response onto dose. Although the pattern of the residual values versus dose suggested a linear relationship, a logarithmic transform was made to obtain a better fit of the data. The equations obtained for each trial are:

Exp. 1: $\log(TLD^{*}) = -1.14 + 1.01 \log(dose)$

Exp. 2: $\log(TLD^{*}) = -1.25 + 1.04 \log(dose)$

Tables 12 and 13 present the values obtained corresponding to the equations above. These values reflect a signficant regression. The change in slope values reflect random changes in the TLD chip or the electronics of the TLD reader response whereas y-intercept values correspond to systematic changes such as the cleanliness of optical system of the TLD reader. The calibration curve for the TLD chips is given in Figure 32.

---

*TLD refers to the sensitivity corrected TLD response.

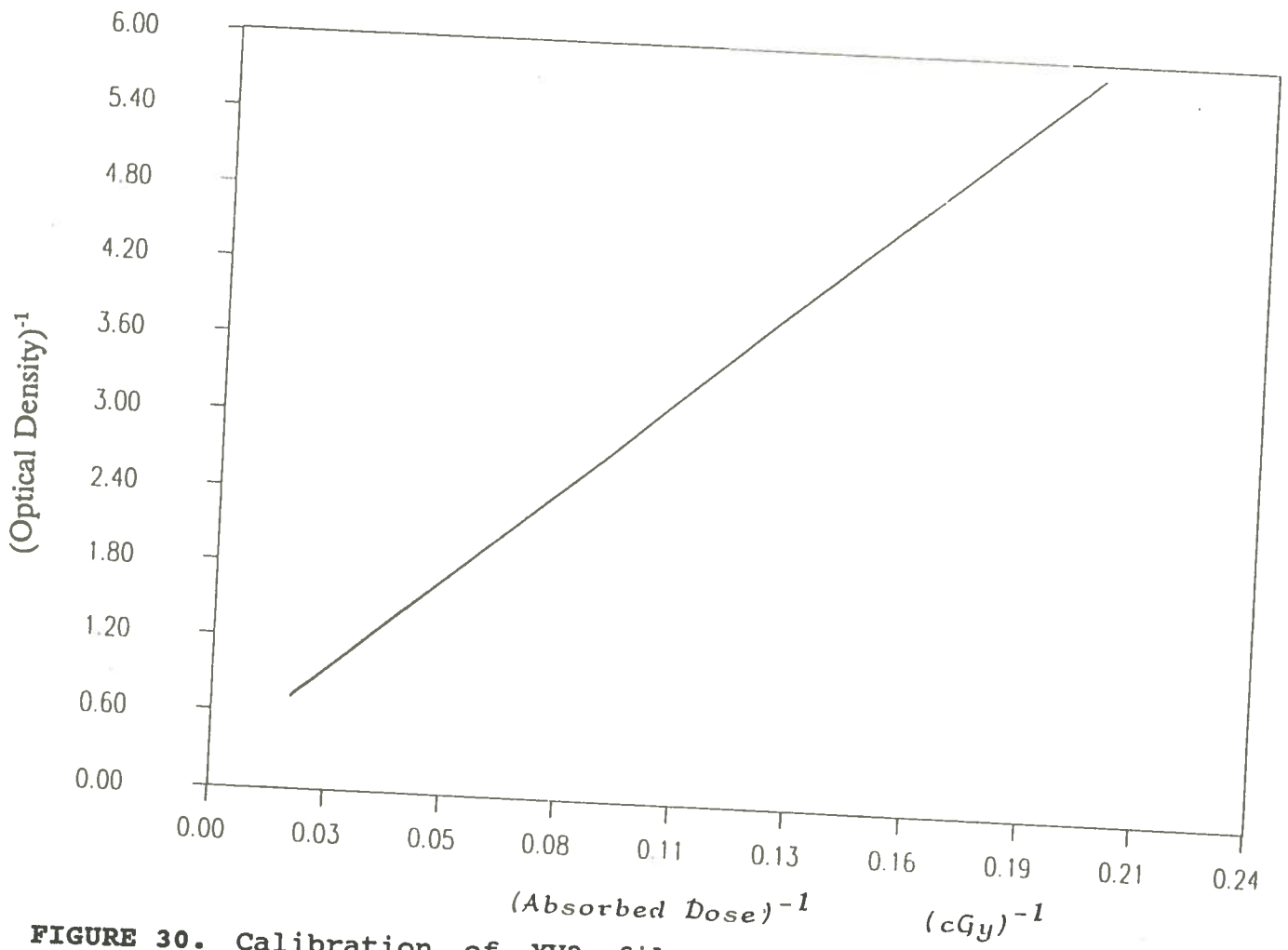

FIGURE 30. Calibration of XV2 film for 9 MeV electrons. A reciprocal transformation of optical density and absorbed dose results in the near superimposition of the two curves representing the two calibrations.

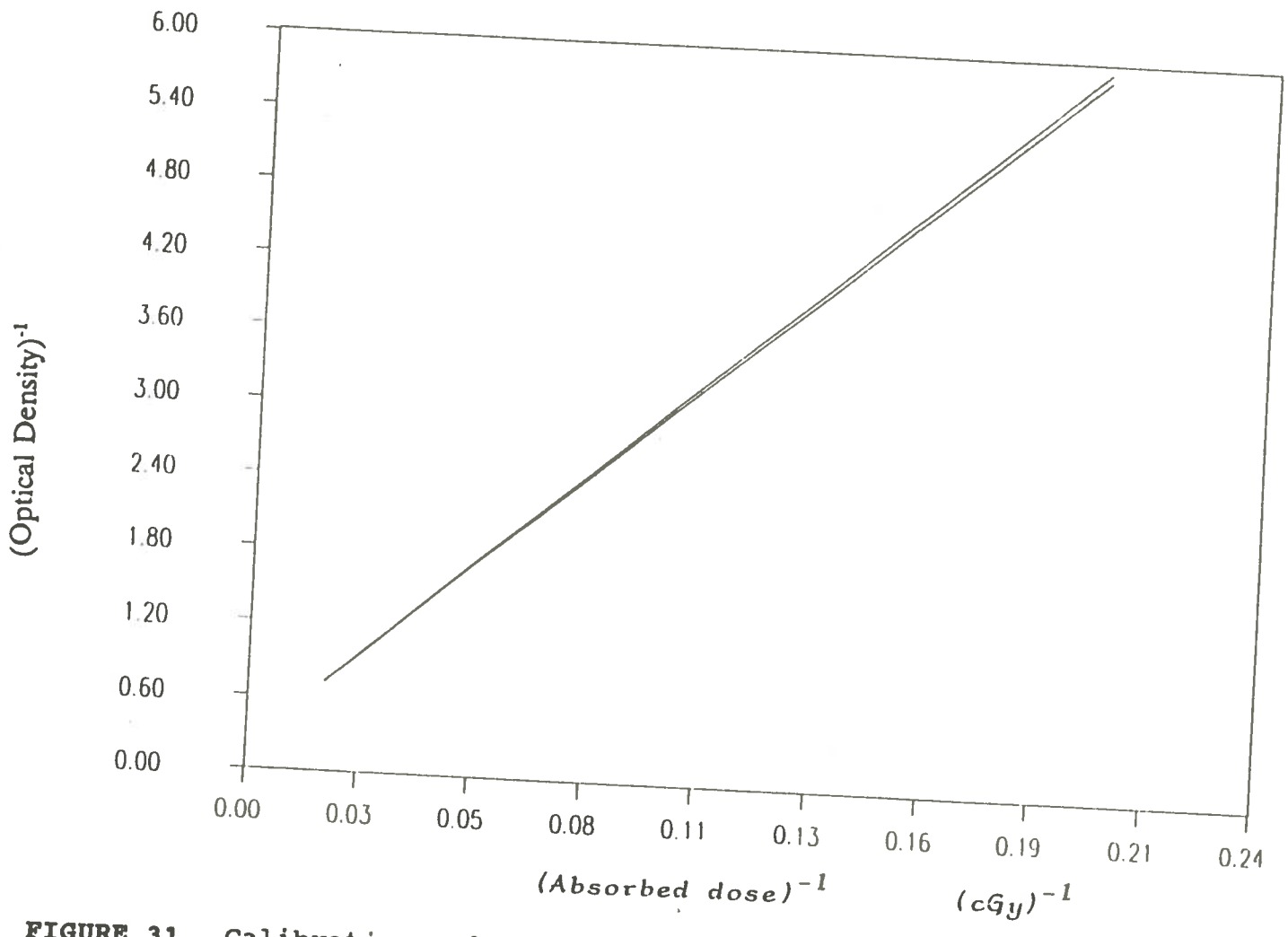

FIGURE 31. Calibration of XV2 film for 6 MeV electrons. A reciprocal transformation of optical density and absorbed dose results in the linearization of data. Two calibrations were performed.

TABLE 13

Statistical parameters determined by the S.A.S./S.T.A.T. program for least squares curve fitting of the sensitivity corrected TLD response onto dose in the calibration of TLD-100 LiF chips. Six (6) MeV electrons.

Parameter	Experiment 1	Experiment 2	% Change
b	-1.143978853	-1.256484483	9.83
m	1.011556902	1.046689040	3.06
r^2	0.999714	0.999762	<-0.01
Pr	0.0001	0.0001	0.00

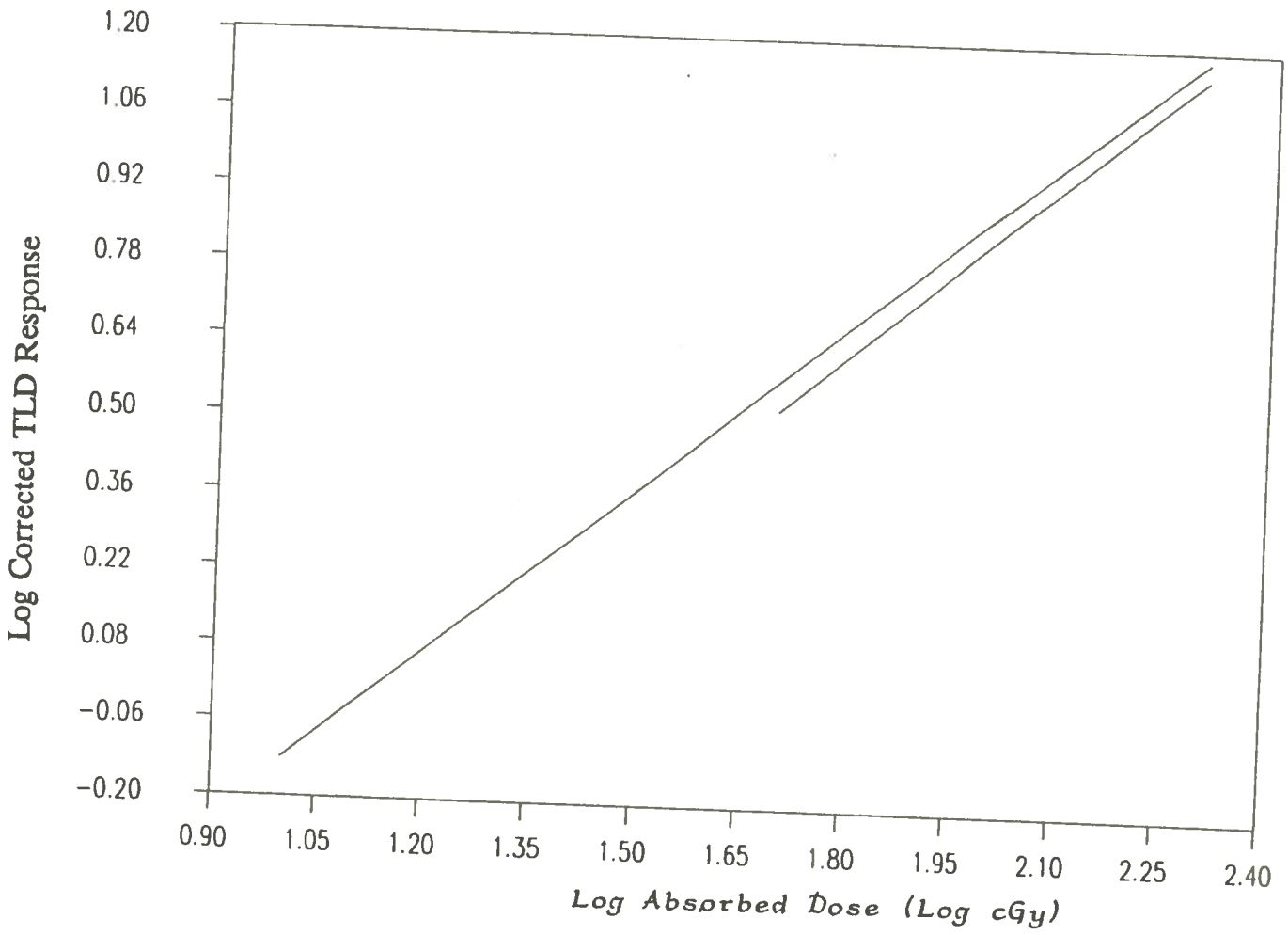

FIGURE 32. Calibration of TLD-100 LiF chips for 6 MeV electrons. A logarithmic transformation of the corrected TLD response and absorbed dose show systematic error. Two calibrations were performed.

3) Variation in the d_{max} Evaluation

The use of the wax-water phantom for the determination of the depth of maximum dose was crude but is required for a complete evaluation of this technique. The exact cutting of a film packet in a darkroom is difficult and the taping of the film packet may cause a density difference between the taped and untaped portions. Based on the ability of the experimenter to cut a perfect circle of film and positioning the film in the phantom, it is difficult to estimate the error. This variation is based on the experimenter's ability and comparison to an actual d_{max} value on a patient was not possible and as such should not be included in an overall error calculation.

4) Overall Error

One value representing the total error of the six dual field technique described in this thesis has been calculated. Presently, there are initial routine weekly TLD evaluation of doses received by patients undergoing total skin electron therapy at Mary Bird Perkins Cancer Center using TLD-100 envelopes placed at various locations on the surface of the patient. Three controls are irradiated to the dose prescribed by the physician for one cycle of treatment. Because TLD chips may be used in the near future, the 5% value has been incorporated into the calculation of overall error. A list of errors that apply to the calculation of an overall error is given in Table 14. The formula for overall error in which the factors are independently related is:

TABLE 14

List of errors applied in the calculation of overall experimental error.

Variation	% Error
Plumb Bob Variation	0.10
Platform Placement Variation	0.25
Phantom Placement Variation	1.50
Ruler Variation	
•in front of scattering panel	0.06
•behind scattering panel	0.33
Gantry Angle Variation	1.09
Acceleration Output	2.00
TLD Variation	5.00
Fractional Contribution of a Single Dual Field	9.00
Output of a Single Dual Field	1.40
Dose Variation Between Positions on a Cylindrical Phantom (good geometry)	11.00

$$overall\ error = \sqrt{a^2 + b^2 + c^2 \ldots n^2}\ .$$

The lower case letters a, b, c, and n refer to the percent errors listed in Table 14. The calculated overall error is 15.4%. The geometry of the patient may give an error of similar magnitude.

CONCLUSIONS

A. Concluding Remarks

The following list of conclusions applies to 9 MeV electrons with the geometries and conditions cited.

1. The adopted formula for the calculation of monitor units required to deliver a precribed dose is acceptable for the six dual field technique investigated in this paper.
2. The unequal $+19^0/-19.6^0$ dual angle produces the most vertically uniform dose in the treatment plane on the Varian Clinac 18 linear accelerator used at Mary Bird Perkins Cancer Center.
3. The output to be used for determining the number of monitor units for the $+19^0/-19.6^0$ dual angle, six dual field technique is 0.0366 cGy/MU.
4. Relative dose values in the treatment plane obtained with the geometry and conditions stated are acceptable when compared to the AAPM Report #23. Kodak XV2 film shows the disuniformity in the treatment plane at all clinically practical points of interest to never rise above 7% nor fall below 10.2% of the value at the calibration point.
5. Water and polystyrene phantom materials yield essentially the same results under the conditions outlined in this study.
6. With source-to-chamber distances on the order of 3 meters in a horizontal beam, the insertion of a 6-mm polystyrene scatterer increases the x-ray contamination of the beam from 2.3 to 3.7%. However, the utilization of

the dual angle reduces the x-ray contamination to that obtained without the scatterer.

7. The output (cGy/MU) is decreased approximately 20% to 0.081 cGy/MU with the insertion of a 6-mm polystyrene scatterer at 3 meters from the source in a horizontal beam. The insertion of the scatterer and beam angulation decreases the output to 0.037 cGy/MU.
8. The insertion of a 6-mm polystyrene scatterer into the horizontal beam at 3 meters decreases the mean incident energy $(\bar{E}_0)$ from 7.4 MeV to 5.5 MeV and remains the same with beam angulation. The presence of the scatterer reduces d_{max}, d_{50}, and R_p values from 1.8 cm, 3.2 cm, and 4.0 cm, respectively, to 1.0 cm, 2.3 cm, and 3.1 cm, and essentially remain the same as the later values with beam angulation.
9. The average value determined for the fractional contribution of one dual field is 0.3445. The greatest variation from the mean is 9%.
10. The total dose to any point with this six dual field technique is delivered from three dual fields.
11. Experiments with the wax-water phantom shows that obliquely incident surfaces are responsible for shifting isodose lines superficially. The d_{max} value with this technique is at least 4 mm in depth versus an average of 9 mm obtained with the flat surfaced phantoms.
12. A series of six dose maxima and minima alternating with a 60-degree periodicity is confirmed with this study.

13. Dosimetric parameters obtained with the electron cones with scattering panels attached shows no significant changes in the values of d_{max}, d_{50}, R_p, $\bar{E}_0$, $\bar{E}_{d_{max}}$ with changes in cone size. The attachment of a polystyrene panel to the cone aperture produces little change in the output (cGy/MU) with the 100 cm SSD geometry.
14. The 100 cm SSD geometry with the attachment of a scatterer to the electron cones shows the values of d_{max}, d_{50}, and R_p to shift superficially roughly equal to the thickness (cm) of the scattering panel.
15. Little difference in the dosimetric parameters is realized with changing the scatter material from polystyrene to acrylic on the electron cone.
16. There is an overall error of 15.4% with this technique.

B. RECOMMENDATIONS

Kodak XV2 film have proven to be a reliable relative dosimetric tool in this study. Although a calibrated ionization chamber is required for absolute measurements, film provides for a quick and accurate evaluation over a large area. Quick evaluation of all beam characteristics at any point is possible using film. A technique for more precise cutting and placement of film within a phantom should be used with future investigations. The use of film between sections of a humanoid phantom may give a more accurate representation of the behavior of the electrons on different areas of the body. A more accurate determination of d_{max} should be made. Overall, however, this study indicates that the use of TLD for patient dosimetry is most practical and more reliable than film and chamber measurements.

The installation of a special high dose rate mode on the linear accelerator which would permit an output of 1 cGy/MU behind the scatterer at 3 meters from the source would be desirable, but may not be financially justified nor operationally practical.

BIBLIOGRAPHY

American Association of Physicists in Medicine (AAPM). *AAPM Report No. 23, Total Skin Electron Therapy: Techniques and Dosimetry.* New York: American Institute of Physics, 1988.

American Association of Physicists in Medicine (AAPM). "A Protocol for the Determination of Absorbed from High-Energy Photon and Electron Beams." *Medical Physics* **10** (1983): 741-771.

Biggs, P.J. "The Effect of Beam Angulation on Central Axis Percent Depth Dose for 4-19 MeV Electrons." *Physics in Medicine and Biology* **29**, No. 9 (1984): 1089-1096.

Bjarngard, B.E., G.T.Y. Chen, R.W. Piontek and G.K. Svensson, "Analysis of Dose Distributions in Whole Body Superficial Electron Therapy." *International Journal of Radiation Oncology, Biology and Physics* **2** (1977): 319-324.

Chase, G.D. and J.L. Rabinowitz. *Principles of Radioisotope Methodology,* 3rd Edition. Minneapolis: Burgess Publishing Company, 1967.

Coffey, C.W., Y. Maruyama, B.L. Stewart and G.A. White. "Electron Beam Irradiation for Mycosis Fungoides Using Variable Energy." *Journal of the Kentucky Medical Association* (July 1982): 398-404.

Cundiff, Jack H. Personal communication. November 1989.

Douglas, A.G. *Evaluation of Photon Contamination in Degraded Electron Beams.* M.S. Thesis, Louisiana State University, 1983.

Dutreix, J. and A. Dutreix. "Film Dosimetry of High Energy Electrons" in "High Energy Radiation Therapy Dosimetry." Ed. J. Laughlin. *Annals of the New York Academy of Science* **161** (1969): 33-43.

Edelstein, G.R., T. Clark and J.G. Holt. "Dosimetry for Total-Body Electron-Beam Therapy in the Treatment of Mycosis Fungoides." *Radiology* **108** (1973): 691-694.

Ekstrand, K.E. and R.L. Dixon. "The Problem of Obliquely Incident Beams in Electron-Beam Treatment Planning." *Medical Physics* **9** (1982): 276-278.

Gastorf, R., L. Humphries, and M. Rozenfeld. "Cylindrical Chamber Dimensions and the Corresponding Values of A_{wall} and $N_{gas} \div N_x A_{ion}$. *Medical Physics* **13**, (1986): 751-754.

Grollman, J.H. Jr., S.M. Bierman, J.E. Morgan, and R.E. Ottoman. "X-Ray Contamination in Total-Skin Electron Therapy of Lymphoma Cutis and Exfoliative Dermatitis." *Radiology* **85** (1965): 356-360.

Habittle, J.L. "A 24 Curie Strontium 90 Unit for Whole-Body Superficial Irradiation with Beta Rays." *British Journal of Radiology* **37**, No. 436 (1964): 297-301.

Holt, J.G., A. Buffa, D.J. Perry, I. Ma, and J.C. McDonald. "Absorbed Dose Measurements Using Parallel Plate Polystyrene Ionization Chambers in Polystyrene Phantoms." *International Journal of Radiation Oncology, Biology and Physics* **5** (1979): 2031-2038.

Holt, J.G. and D.J. Perry. "Some Physical Considerations in Whole Skin Electron Beam Therapy." *Medical Physics* **9**, No. 5 (1982): 769-776.

International Commission on Radiation Units and Measurements (ICRU). *ICRU Report No. 35, Radiation Dosimetry: Electron Beams with Energies Between 1 and 50 MeV.* Bethesda, MD: ICRU, 1984.

Karzmark, C.J. "Large-Field Superficial Electron Therapy with Linear Accelerators." *British Journal of Radiology* **37**, No. 436 (1964): 302-305.

Karzmark, C.J., R. Loevinger, R.E. Steel and M. Weisbluth. "A Technique for Large-Field Superficial Electron Therapy." *Radiology* **74** (1960): 633-644.

Karzmark, C.J. and R.J. Morton. *A Primer on Theory and Operation of Linear Accelerators in Radiation Therapy.* U.S. Department of Health and Human Services. Bureau of Radiological Health Publication No. FDA82-8181. Rockville, MD: Bureau of Radiological Health, 1981.

Kumar, P.P., R.R. Good and E.O. Jones. "Dosimetry of Rotational Versus Multifield Total-Skin Electron-Beam Therapy [TSEBT] Techniques." *Radiation Medicine* **5**, No. 2 (1987): 51-54.

Kumar, P.P., U.K. Henschke, K.P. Mandal, J.R. Nibhanupudy and I.S. Patel. "Early Experience in Using an 18 MeV Linear Accelerator for Mycosis Fungoides at Howard University Hosptial." *Journal of the National Medical Association* **69**, No. 4 (1977): 223-226.

Loevinger, R., C.J. Karzmark, and M. Weissbluth. "Radiation Therapy with High-Energy Electrons." *Radiology* **35** (1961): 906-927.

Mota, H.C., C.H. Sibata, W. Roberts and P.D. Higgins. "Film Dosimetry: Linearization of Dose-Response for Relative Measurements of Dose Distribution." *Physics in Medicine and Biology* **35**, No. 4 (1990): 565-570.

Niroomand-Rad, A., M.T. Gillian, R. Komaki, R.W. Kline and D.F. Grimm. "Dose Distribution in Total Skin Electron Beam Irradiation Using the Six-Field Technique." *International Journal of Radiation Oncology Biology and Physics* **12** (1986): 415-419.

Page, V., A. Gardner, and C.J. Karzmark. "Patient Dosimetry in the Electron Treatment of Large Superficial Lesions." *Radiology* **94** (1970): 635-641.

SAS Institute, Inc. *SAS/STAT Guide for Personal Computers, Version Edition.* Cary, NC: SAS Institute Inc., 1985. 378 pp.

Sewchand, W., F.M. Khan, and J. Williamson. "Total-Body Superficial Electron-Beam Therapy Using a Multiple-Field Pendulum-Arc Technique." *Radiology* **130** (1979): 493-498.

Smith, Susan. Personal communication. 11 November 1989.

Szur, L., J.A. Silvester, and D.K. Bewley. "Treatment of the Whole Body Surface with Electrons." *The Lancet* **1** (1962): 1373-1377.

Tetenes, P.J. and P.N. Goodwin. "Comparative Study of Superficial Whole-Body Radiotherapeutic Techniques Using a 4-MeV Nonangulated Electron Beam." *Radiology* **122** (1977): 219-226.

Trump, J.G., K.A. Wright, W.W. Evans, J.H. Anson, H.F. Hare, J.L. Fromer, G. Jacque and K.W. Horne. "High Energy Electrons for the Treatment of Extensive Superficial Malignant Lesions." *American Journal of Roentegenology* **69** (1953): 623-629.

Vonderheid, E.C. and Micaily, B. "Cutaneous T-Cell Lymphoma." *Principals and Practice of Radiation Oncology*. Eds., C.A. Perez and L.W. Brady. Philadelphia: J.B. Lippincott, 1987. 1316 pp.

White, C.A. *A Methodological Evaluation of the Energies in Degraded Electron Beams.* M.S. Thesis, Louisiana State University, 1983.

Zimmerman, D.W., C.R. Rhyner and J.R. Cameron. Thermal Annealing Effects on the Thermoluminescence of LiF. *Health Physics* **12** (1966): 525-531.

VITA

Jeffrey Paul Kurr was born on September 10, 1954, in Fairfield, Illinois. He attended Fairfield Community High School in Fairfield and graduated in May, 1972. In 1978, he obtained a Bachelor of Science Degree in Radiologic Technology from Northeast Louisiana University in Monroe, Louisiana. Following graduation he was employed at St. Francis Medical Center in Monroe, and attended Northeast Louisiana University pursuing a graduate degree in Geosicence. He entered graduate school and received a graduate assistantship in the Nuclear Science Center at Louisiana State University in August, 1987. In August, 1988, his assistantship duties and training were centered at Mary Bird Perkins Cancer Center. He is currently a candidate for the Master of Science Degree in Nuclear Science, Medical Radiation Science Option, and is employed at Mississippi Baptist Medical Center, Jackson, Mississippi.

EXAMINATION AND THESIS REPORT

Candidate: Jeffrey Paul Kurr

Major Field: Nuclear Science

Title of Thesis: A Study on the 9-MeV Total Skin Electron Therapeutic Technique

Approved:

Oscar Hidalgo S.
Major Professor and Chairman

Dean of the Graduate School

EXAMINING COMMITTEE:

Edward V. Hungerford

Carrie M. Lucas

Date of Examination:

April 19, 1991